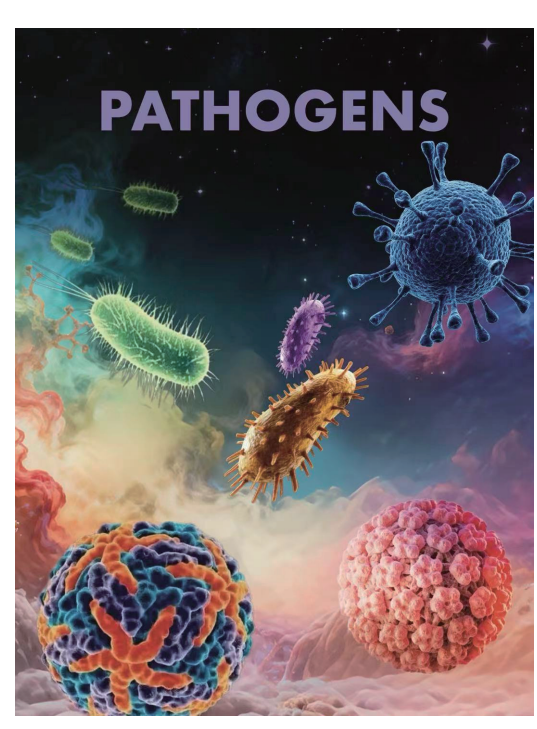
CHINA CDC WEEKLY

Vol. 7 No. 43 Oct. 24, 2025 Weekly

中国疾病预防控制中心周报



Commentary

Salmonella enterica ST8333 Was Isolated as Early as July 2015

1347

Vital Surveillances

Epidemiological Characteristics and Spatiotemporal Clustering Analysis of Human Rabies

— China, 2005–2024

1350

Genomic Characterization of Human Adenovirus Type 21 Strains — 7 PLADs, China, 2023–2024

1357

Preplanned Studies

Detection of Dengue Virus RNA in Breast Milk Following Peripartum Infection — Guangzhou City, Guangdong Province, China, 2024

1364

Prospective Study on Clinical Performance of Host DNA Methylation Assay for Triage in Women Who Are HPV-Positive — 4 Provinces, China, 2018–2021

1368







China CDC Weekly

Editorial Board

Editor-in-Chief Hongbing Shen **Founding Editor** George F. Gao

Deputy Editor-in-Chief Liming Li Gabriel M Leung Zijian Feng

Executive Editor Chihong Zhao **Members of the Editorial Board**

Wen Chen Xi Chen (USA) Zhuo Chen (USA) Rui Chen Ganggiang Ding Xiaoping Dong Pei Gao Mengjie Han Yuantao Hao Na He Yuping He Guoqing Hu Zhibin Hu Weihua Jia Yuegin Huang Na Jia Zhongwei Jia Guangfu Jin Xi Jin Biao Kan Haidong Kan Ni Li Qun Li Ying Li Zhenjun Li Min Liu Qiyong Liu Xiangfeng Lu Jun Lyu Huilai Ma Jiagi Ma Chen Mao Ron Moolenaar (USA) An Pan Xiaoping Miao Daxin Ni Lance Rodewald (USA) William W. Schluter (USA) Yiming Shao Xiaoming Shi Yuelong Shu RJ Simonds (USA) Xuemei Su Chengye Sun Quanfu Sun Xin Sun Feng Tan **Jinling Tang Huaging Wang** Hui Wang **Linhong Wang Tong Wang** Guizhen Wu Jing Wu Xifeng Wu (USA) Yongning Wu Min Xia Ningshao Xia Yankai Xia Lin Xiao Dianke Yu Hongyan Yao Zundong Yin Hongjie Yu Shicheng Yu Ben Zhang Jun Zhang Liubo Zhang Wenhua Zhao Yanlin Zhao Xiaoying Zheng Maigeng Zhou Xiaonong Zhou Guihua Zhuang

Advisory Board

Director of the Advisory Board Jiang Lu

Vice-Director of the Advisory Board Yu Wang Jianjun Liu Jun Yan

Members of the Advisory Board

Chen Fu Gauden Galea (Malta) Dongfeng Gu Qing Gu Yan Guo Ailan Li Jiafa Liu Peilong Liu Yuanli Liu Kai Lu Roberta Ness (USA) **Guang Ning** Minghui Ren Chen Wang Hua Wang Kean Wang Xiaoqi Wang Zijun Wang Fan Wu Xianping Wu

Jingjing Xi Jianguo Xu Gonghuan Yang Tilahun Yilma (USA)

Guang Zeng Xiaopeng Zeng Yonghui Zhang Bin Zou

Editorial Office

Directing Editor Chihong Zhao
Managing Editors Yu Chen

Senior Scientific Editors Daxin Ni Ning Wang Wenwu Yin Jianzhong Zhang Qian Zhu

Scientific Editors

Weihong Chen Tao Jiang Xudong Li Nankun Liu Liwei Shi Liuying Tang Meng Wang Zhihui Wang Qi Yang Qing Yue Lijie Zhang Ying Zhang

Cover Image: credited from the designer Jiaying Wang.

Commentary

Salmonella enterica ST8333 Was Isolated as Early as July 2015

Yanan Wang^{1,2,#}; Yue Liu³; Baoli Zhu⁴; George F. Gao^{4,5}; Xuebin Xu^{3,#}

We read the study conducted by Cui et al. published in *China CDC Weekly* with great interest, and would like to make comment on this matter (1). The report identified 31 *Salmonella enterica* serovar I 1,4,[5],12:i:- (S. I 1,4,[5],12:i:-) sequence type 8333 (ST8333) genomes by the end of 2023 in the National Molecular Tracing Network for Foodborne Disease Surveillance database. The overall percentage of isolates of *S.* I 1,4,[5],12:i:- ST8333 remained low in their active monitoring between 2017 and 2023, and observed ST8333 in 2017.

In fact, ST8333 was first assigned in the EnteroBase database (https://enterobase.warwick.ac.uk/) based on 7 housekeeping genes (including aroC: 10, dnaN: 19, hemD: 1050, hisD: 9, sucA: 9, purE: 5, and thrA: 2) on January 15, 2021 (Figure 1A) (2). The first S. I 1,4,[5],12:i:- ST8333 strain was isolated from a case of sporadic diarrhea (a 1-year-old girl) in the Xinjiang Uygur Autonomous Region, China, on August 24, 2017 (2). In our previous study, we built an openaccess Chinese Local Salmonella Genome Database version 2 (CLSGDB v2, https://nmdc.cn/clsgdbv2), which consisted of 7,997 high-quality genomes with 164 serovars and 295 STs, including two S. I 1,4,[5],12:i:- ST8333 genomes (3). In addition to our previous report (2), another S. I 1,4,[5],12:i:- ST8333 strain was isolated from frozen raw ground pork in Hanzhong City, Shaanxi Province, China in August 2019 (3). Cui et al. reported 31 ST8333 genomes from 4 provincial-level administrative divisions (PLADs) in China, thereby increasing the knowledge of the prevalence and distribution of ST8333 (1). Based on our recent sequencing data and mining of publicly available databases as of June 12, 2025 (including NCBI, Enterobase, and CLSGDBv2) (3), we found that S. I 1,4,[5],12:i:- ST8333 was isolated from a 1year-old boy in Xinjiang as early as July 25, 2015. Therefore, we depicted the timeline of ST8333 for its existence and discovery to help us better understand the spread of this important ST (Figure 1A). According to the date of isolation, at least six S. I 1,4,[5],12:i:-ST8333 isolates had existed in Xinjiang before 2017. Three of these were isolated from children under 5

years of age.

Based on the phylogenetic analysis of 31 S. I 1,4,[5],12:i:- ST8333 genomes, Cui et al. concluded that the ST8333 strain originated in Qinghai Province in 2017 and then spread to Xinjiang, Sichuan, and Jiangsu PLADs, China (1). However, because of the limited genomic data used, their conclusions may exist certain limitations in terms of accuracy. Our analysis indicated that endemic transmission (the presence of a like-outbreak) occurred in Xinjiang in July 2015, and then spread to other PLADs, such as Sichuan and Shaanxi (Figure 1B). These findings suggest that the location where the ST8333 strain was first isolated does not necessarily represent the location where the ST first appeared. In addition, due to the limited release of the genomic data (1), we were unable to conduct comparative genomic analyses to obtain a better evolutionary analysis. Therefore, we recommend further data sharing as soon as possible.

Further *in silico* analysis showed a total of 124 acquired antibiotic resistance genes (ARGs); 6 strains carried third-generation cephalosporin resistance genes, including *bla*_{CTX-M-65} and *bla*_{CTX-M-55}, and 5 strains carried the fluoroquinolone resistance gene *qnrS1*. Very few ARGs, plasmid replicons, and mobile genetic elements (MGEs) were identified in earlier isolates (i.e., 2015) compared to genomes isolated in recent years (Figure 1B). The co-existence of several ARGs (*qnrS1*, *bla*_{OXA-10}, *bla*_{CTX-M-65}, *cmlA1*, *lun(F)*, *dfrA14*, and *ARR-2*), IncHI2 replicon, and MGEs (IS*102*, IS*5075*, IS*1006*, IS*Ror7*, IS*Kpn8*, and IS*Kpn19*) in strains isolated in 2021 and 2022 was observed (Figure 1B).

Recently, S. I 1,4,[5],12:i:- has become the most prevalent cause of human infections in China, and ST34 is the predominant ST among human infection cases in China (1,3). Comparative genomics confirmed that ST8333 evolved from S. I 1,4,[5],12:i:-ST34 (2), which is prone to multidrug resistance (MDR). Based on limited data, the number of infection cases caused by ST8333 is increasing, and the ST8333 strain has become increasingly severe owing to the acquisition of ARGs. It remains uncertain whether ST8333 will

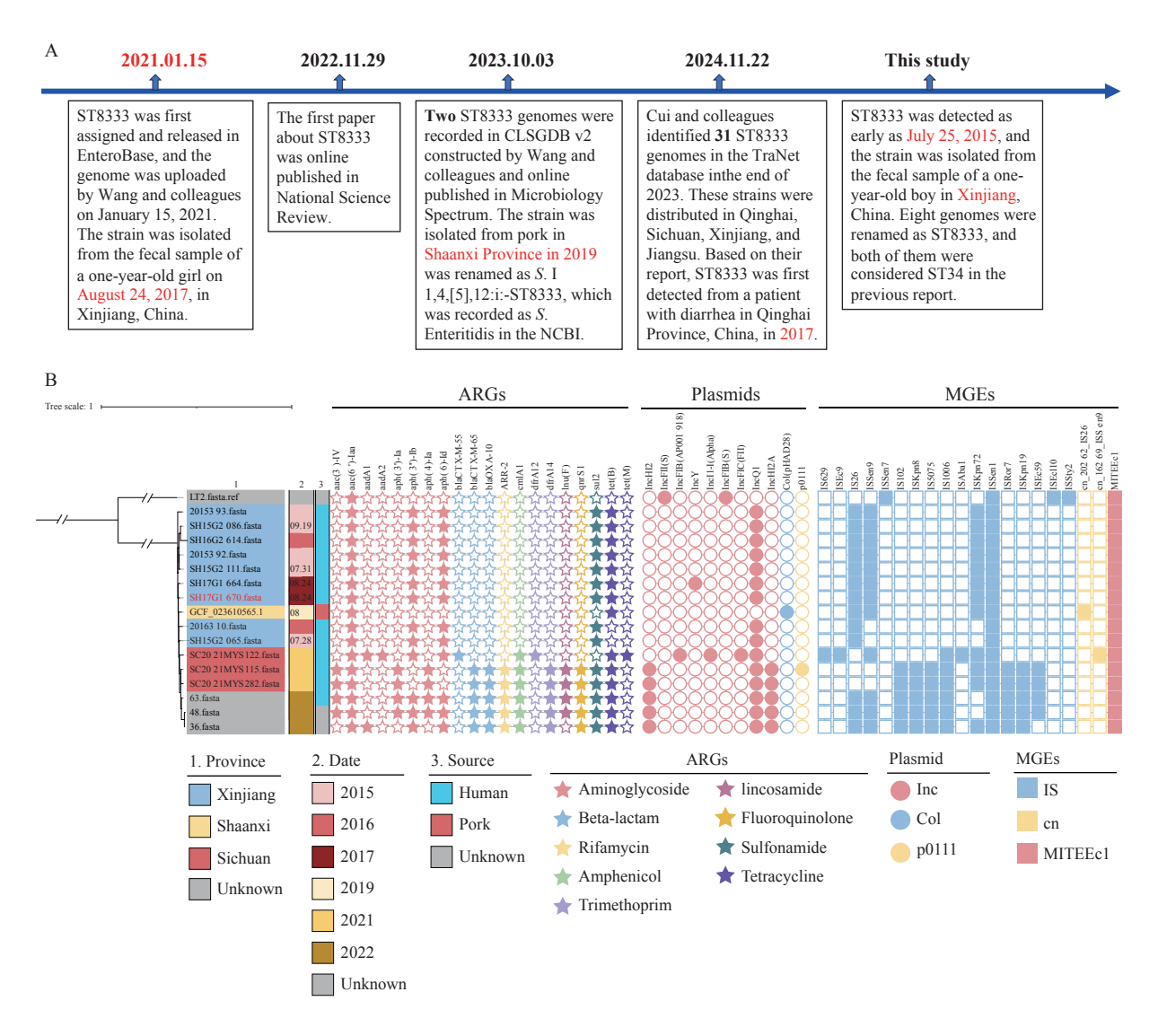


FIGURE 1. Discovery timeline and phylogenetic analysis of S. I 1,4,[5],12:i:- ST8333. (A) Timeline of ST8333 for its existence and discovery; (B) Phylogenetic analysis of S. I 1,4,[5],12:i:- ST8333 genomes.

Note: Four strains, including DS23IMWYN 873, SH17G1670, SH15G2065, and SH15G2086, were isolated from children under 5 years old; SH15G2111 and SH17G1664 were isolated from 17 and 35 years old, respectively; the others were unknown. The core genome phylogeny and multi-alignments were performed using the Parsnp v2.1.0 (https://github.com/marbl/parsnp) and visualized using the Interactive Tree of Life (iTOL version 7.0, https://itol.embl.de/). 2015393: SAMN35670174; 2015392: SAMN35670173; SH15G2065: SAMN35670843; SH15G2086: SAMN35670847; SH15G2111: SAMN35670848; 2016310: SAMN35670191; SH16G2614: SAMN35680157; SH17G1664: SAMN35680386; SH17G1670: SAL_FB7519AA (SAMN21890000); 36: SAL_PB8236AA; 48: SAL_PB8237AA; 63: SAL_OB7431AA; SAL_NB5708AA: SC2021MYS115: SAL NB5716AA; SC2021MYS122: SC2021MYS282: SAL NB5698AA. DS23IMWYN237 870: SAMN48529803. For (A), the timeline in the diagram briefly describes the significant stories at each time point. For (B), location, collection date, isolation source, ARGs, plasmid replicons, MGEs, and SPIs are indicated with different colors and shapes, respectively.

Abbreviation: ARGs=antibiotic resistance genes; MGEs=mobile genetic elements; SPIs=Salmonella Pathogenic Islands.

replace ST34 as the primary sequence type clone that causes human infections worldwide. These findings highlight the need for global public health attention and urgent genomic monitoring.

The emergence and increasing trends of antimicrobial resistance (AMR) worldwide are among the top 10 public health threats (4). S. enterica is listed

on the 2024 World Health Organization Bacterial Priority Pathogens List (5–6), and the increasing trends of AMR in *S. enterica* are of great public health concern (2–3,7). With recent advances in large dataempowered artificial intelligence (AI) and machine learning, WGS has become critical for tracking the rapid spatiotemporal evolution of AMR in *S. enterica*

(2-3,7-11). These findings underscore the importance of high-quality, open-access regional and international genomic databases for fighting against AMR, ARGs, and informing outbreak response (11-12). Therefore, more publicly available data on S. I 1,4,[5],12:i:- and S. Typhimurium will help to better evaluate the spread situation in real-time and enable the scientific community to formulate and adjust prevention and control policies in a prompt manner. Failure to fill these gaps may lead to underestimation of the risk of transmission of the MDR ST8333 clone and the emergence of new variants in S. I 1,4,[5],12:i:-. Considering the positive correlation between the gross output of meat, population density, annual mean temperature, and AMR in Salmonella (3,7), as well as the emergence of MDR ST8333 in meat (pork), we call for more S. I 1,4,[5],12:i:- and S. Typhimurium strains from meat and animal sources for WGS and data sharing in the open-access Salmonella genome database.

Conflicts of interest: The views and claims in published articles are those of the authors and do not represent any viewpoint from the *China CDC Weekly*.

Acknowledgements: The Veterinary Big Data and Bioinformatics Center, Henan Agricultural University, for their support and help.

Funding: Supported in part by grants from the Project for the National Key Research and Development Program of China (2023YFC2307101), Young Scientist of the Joint Funds of Science and Technology Research and Development Plan of Henan Province, China (235200810058), and Young TopNotch Talents Foundation of Henan Agricultural University (30501278).

doi: 10.46234/ccdcw2025.226

* Corresponding authors: Yanan Wang, wangyanan1001@henau. edu.cn; Xuebin Xu, xuxuebin@scdc.sh.cn.

Copyright © 2025 by Chinese Center for Disease Control and Prevention. All content is distributed under a Creative Commons Attribution Non Commercial License 4.0 (CC BY-NC).

Submitted: June 13, 2025 Accepted: September 29, 2025 Issued: October 24, 2025

REFERENCES

- Cui QP, Yang XR, Yang TT, Wang X, Ma X, Liu YX, et al. Characterization and implications of the regionally prevalent ST8333 strains of Salmonella enterica serotype 4,[5],12:i: — China, 2017–2023.
 China CDC Wkly 2024;6(47):1232 – 5. https://doi.org/10.46234/ccdcw2024.247.
- 2. Wang YN, Liu Y, Lyu N, Li ZY, Ma SF, Cao DM, et al. The temporal dynamics of antimicrobial-resistant *Salmonella enterica* and predominant serovars in China. Natl Sci Rev 2023;10(3):nwac269. https://doi.org/10.1093/nsr/nwac269.
- 3. Wang YN, Xu XB, Zhu BL, Lyu N, Liu Y, Ma SF, et al. Genomic analysis of almost 8,000 *Salmonella* genomes reveals drivers and landscape of antimicrobial resistance in China. Microbiol Spectr 2023;11(6):e02080 23. https://doi.org/10.1128/spectrum.02080-23.
- 4. Xiao YH, Nishijima T. Status and challenges of global antimicrobial resistance control: a dialogue between Professors Yonghong Xiao and Takeshi Nishijima. hLife 2024;2(2):47 9. https://doi.org/10.1016/j. hlife.2023.11.004.
- WHO. WHO bacterial priority pathogens list, 2024: bacterial pathogens of public health importance to guide research, development and strategies to prevent and control antimicrobial resistance. Geneva: World Health Organization; 2024.
- Ma YY, Chen P, Mo Y, Xiao YH. WHO revised bacterial priority pathogens list to encourage global actions to combat AMR. hLife 2024;2(12):607 – 10. https://doi.org/10.1016/j.hlife.2024.10.003.
- Wang YN, Xu XB, Jia SL, Qu MQ, Pei YH, Qiu SF, et al. A global atlas and drivers of antimicrobial resistance in *Salmonella* during 1900-2023. Nat Commun 2025;16(1):4611. https://doi.org/10.1038/ s41467-025-59758-3.
- Baker S, Thomson N, Weill FX, Holt KE. Genomic insights into the emergence and spread of antimicrobial-resistant bacterial pathogens. Science 2018;360(6390):733 – 8. https://doi.org/10.1126/science. aar3777.
- Mather AE, Gilmour MW, Reid SWJ, French NP. Foodborne bacterial pathogens: genome-based approaches for enduring and emerging threats in a complex and changing world. Nat Rev Microbiol 2024;22(9):543 – 55. https://doi.org/10.1038/s41579-024-01051-z.
- Xiang Y, Zhu KP, Min KY, Zhang YW, Liu JF, Liu KK, et al. Characterization of a Salmonella enterica serovar Typhimurium lineage with rough colony morphology and multidrug resistance. Nat Commun 2024;15(1):6123. https://doi.org/10.1038/s41467-024-50331-y.
- Wang YN, Xu XB, Zhu BL, Gao GF. Enhanced genomic surveillance is essential for effective *Salmonella* outbreak response. China CDC Wkly 2025;7(26):880 – 881. https://doi.org/10.46234/ccdcw2025.151.
- Zheng BW, Liu Y, Xiao YH, Harnessing a high-quality Salmonella genome catalog to combat antimicrobial resistance and inform outbreak responses. Biosaf Health 2025. https://doi.org/10.1016/j.bsheal.2025. 09.009.

International Joint Research Center of National Animal Immunology, College of Veterinary Medicine, Henan Agricultural University, Zhengzhou City, Henan Province, China; ² Longhu Laboratory of Advanced Immunology, Zhengzhou City, Henan Province, China; ³ Division of Pathogen Testing and Analysis, Shanghai Municipal Center for Disease Control and Prevention, Shanghai, China; ⁴ CAS Key Laboratory of Pathogen Microbiology and Immunology, Institute of Microbiology, Chinese Academy of Sciences, Beijing, China; ⁵ Chinese Center for Disease Control and Prevention, Beijing, China.

Vital Surveillances

Epidemiological Characteristics and Spatiotemporal Clustering Analysis of Human Rabies — China, 2005–2024

Xi Chen¹; Jinhui Zhang¹; Shouming Lyu²³; Canjun Zheng⁴; Wenwu Yin⁴; Di Mu⁴♯; Yanping Zhang⁴

ABSTRACT

Introduction: Rabies remains a significant zoonotic disease in China. Following comprehensive control measures implemented since 2006, annual human cases declined steadily from 2008 through 2023. However, 2024 witnessed a 36.9% increase in cases compared with 2023, indicating possible changes in transmission dynamics or control effectiveness. This study analyzes the epidemiological characteristics and spatiotemporal patterns of rabies from 2005 to 2024 to inform targeted prevention strategies.

Methods: We employed descriptive epidemiological methods to analyze the spatiotemporal distribution and demographic characteristics of rabies cases in China. Spatial clustering was assessed using global and local Moran's I statistics (*P*<0.05). Retrospective space-time scan analysis (2005–2024) was performed using SaTScan software to identify significant disease clusters. We conducted spatial frequency analysis by calculating the number of years each county reported at least one case during the study period; counties reporting cases in ≥10 years were classified as high-frequency areas.

Results: Following a peak of 3,300 cases in 2007, rabies incidence declined continuously for 16 years before resurging in 2024 (167 cases, representing a 36.9% increase compared with 2023). Cases remained geographically concentrated, with 76.0% occurring in six central and southern provincial-level administrative divisions. The majority of affected counties (74%) reported only a single case. Males (70.0%), farmers (68.6%), and individuals aged 41-70 years (53.8%) comprised the highest-risk populations. Spatial analysis revealed that High-High clusters decreased in number over time. These clusters also shifted geographically: from widespread distribution across southwestern provincial-level administrative divisions (PLADs) during 2005-2014 to concentration in central agricultural zones during 2020-2024, particularly along the border regions of Henan, Hunan, Hubei,

and Anhui PLADs. We identified 352 high-frequency counties. Spatiotemporal scan statistics detected seven significant clusters during 2005–2024, all located in central and southwestern regions. Outbreaks within these clusters peaked during summer and autumn months (July–November) from 2006 to 2013, with no new clusters emerging after 2014.

Conclusions: Our findings demonstrate that China's rabies control efforts have successfully transitioned the epidemic from widespread endemic transmission to sporadic occurrence with localized clustering. The 2024 resurgence occurred predominantly in historically endemic hotspots identified through spatial analysis. Sustaining these control achievements will require implementing precision prevention strategies specifically targeted at these persistent high-risk counties.

Rabies remains a critical public health concern, with a near-100% fatality rate once the virus infects the central nervous system and clinical symptoms emerge (1). Globally, approximately 59,000 deaths attributable to rabies occur annually (2). During the 1970s–1980s, China experienced several thousand human rabies cases each year, representing a substantial public health burden (3). To combat this threat, China implemented comprehensive control measures in the 20th century, focusing primarily on canine population management. By the late 1990s (1995–1999), annual case counts had declined to approximately 230, nearing levels considered manageable for public health systems (4). However, the epidemic subsequently resurged rapidly, peaking at 3,300 cases in 2007 (3).

Since 2006, the Chinese government implemented a series of comprehensive prevention and control measures against rabies. These measures include strengthening human rabies surveillance, conducting outbreak containment and source elimination campaigns, enhancing the and

management and vaccination of domestic dogs (5). Additionally, China has issued several key technical guidelines, including the *Guidelines for the Management of Rabies Exposure Prophylaxis* (2006, 2009, and 2023 editions) and the *Guidelines for the Diagnosis and Treatment of Rabies* (2021 edition) (6). From 2008 to 2023, China achieved 16 consecutive years of declining human rabies incidence, reaching a historic low of 122 cases in 2023 (7) — the lowest level recorded since 1950. However, in 2024, the country reported 167 human rabies cases, representing a 36.9% increase compared to 2023. This resurgence may reflect changes in transmission dynamics, gaps in current control measures, or both.

A systematic analysis of the spatiotemporal heterogeneity of rabies transmission following these epidemiological changes is urgently needed to identify current gaps in rabies control. This study employs spatial autocorrelation analysis and spatiotemporal scan statistics on national rabies surveillance data (2005–2024) to: 1) characterize spatiotemporal evolution patterns over two decades; 2) identify highrisk space-time clusters; and 3) pinpoint vulnerable areas requiring strengthened interventions. These findings will provide critical evidence to support China's goal of eliminating dog-mediated human rabies by 2030.

METHODS

Data Sources

National rabies surveillance data for laboratory-confirmed and clinically diagnosed human cases from 2005 to 2024 were obtained from the China CDC Information System, encompassing 31 provincial-level administrative divisions (PLADs) in China. Each case record included the date of symptom onset and the patient's residential address at the county level.

Statistical Methods

We employed descriptive epidemiological methods to systematically characterize the temporal, spatial, and demographic patterns of rabies cases in China. Temporal trends were visualized through annual incidence curves. Spatial analysis comprised three components: 1) Calculation of global and local Moran's I indices to identify statistically significant (*P*<0.05) spatial clusters (hotspots and coldspots). 2) Retrospective space-time scan analysis using SaTScan v9.3, applying a discrete Poisson model to

monthly case data (2005–2024). The circular scanning window was configured with a maximum spatial cluster radius of 500 km, and cluster significance was assessed through 999 Monte Carlo simulations (8). 3) Spatial frequency analysis, in which each county was assigned an occurrence score based on the number of years (out of 20 total study years) in which at least one case was reported, yielding scores ranging from 0 to 20. Counties with scores exceeding 10 (indicating case reports in more than half of the study period) were classified as high-frequency counties. All statistical analyses were performed using R software (version 4.3.2; R Foundation for Statistical Computing, Vienna, Austria), with a significance threshold of $\alpha = 0.05$.

RESULTS

Epidemiological Overview

Between 2005 and 2024, China reported 24,746 human rabies cases. The epidemic reached its peak in 2007 with 3,300 cases, followed by a rapid decline from 2008 through 2019. During 2020–2023, the rate of decline decelerated substantially, reaching a historic low of 122 cases in 2023 — the lowest annual incidence recorded since 1950. However, 2024 witnessed 167 reported cases, marking a 36.9% increase compared to the previous year. This represented the first resurgence following 16 consecutive years of decline, though case numbers remained considerably lower than those observed during 2005–2019 (Figure 1).

Human Rabies Distribution in 2024

The 167 human rabies cases reported in 2024 were distributed across 122 counties in 20 PLADs. Six PLADs accounted for 76.0% of all cases: Henan (49 cases), Guangxi (22 cases), Hunan (19 cases), Hubei (13 cases), Anhui (12 cases), and Jiangsu (12 cases). At the county level, 91 counties (74.5%) reported a single case, while 23 counties (18.8%) reported 2 cases. Additionally, 4 counties reported 3 cases, 3 counties reported 4 cases, and 1 county reported 5 cases. These higher-incidence counties were primarily located in Henan (5 counties), Guangxi (2 counties), and Hubei (1 county).

Year-on-Year Comparison (2023–2024)

Henan demonstrated the highest absolute increase (14 additional cases) and the greatest number of

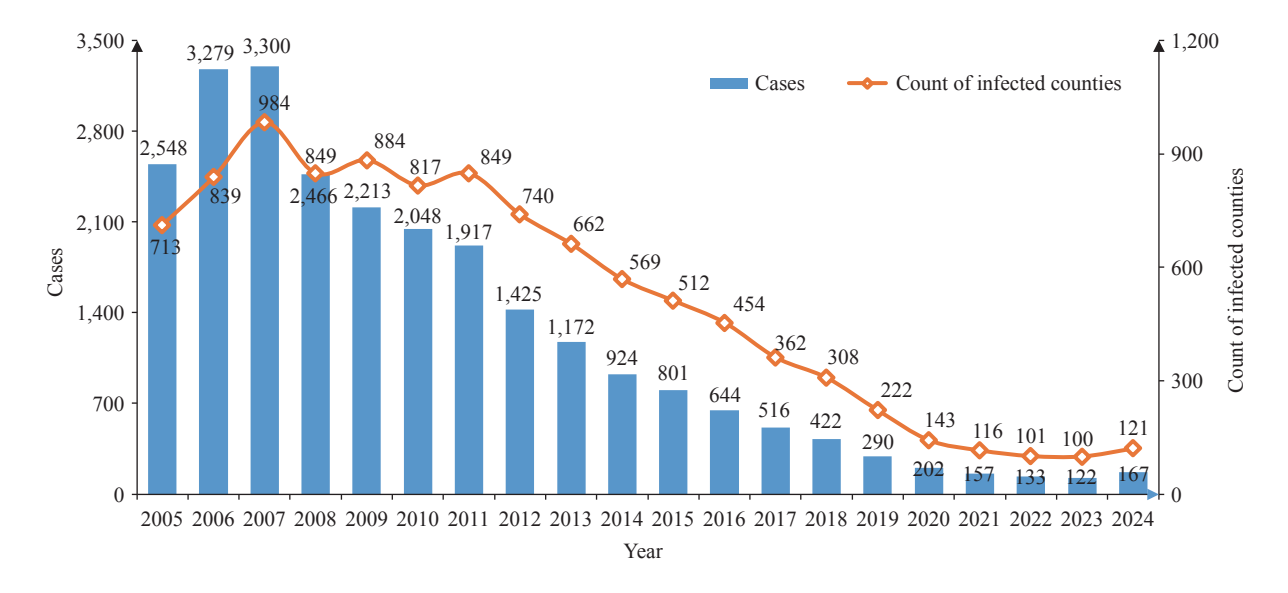


FIGURE 1. Time-series analyses of human rabies in China, 2005–2024.

affected counties [27 total reporting counties, with 18 (66.7%) showing rising case numbers]. Other PLADs with notable increases included Guangxi (5 counties, +11 cases), Jiangsu (5 counties, +7 cases), Hubei (3 counties, +7 cases), and Guizhou (5 counties, +6 cases). Five counties reported their first cases since 2005: Shenzhou (Hebei), Siyang (Jiangsu), Cixi (Zhejiang), Shilong (Henan), and Baojing (Hunan) (Table 1).

Spatial Autocorrelation Analysis

We conducted global and local spatial clustering analyses on five-year average incidence rates of human rabies in China from 2005 to 2024. Global spatial autocorrelation: Across all study periods (2005–2009, 2010–2014, 2015–2019, and 2020–2024), Moran's I values exceeded zero with *P*<0.05, demonstrating statistically significant spatial clustering and positive spatial autocorrelation in disease distribution patterns.

Local Spatial Autocorrelation

During 2005–2009, we identified 130 high-high cluster counties, primarily concentrated in Guangxi, Guangdong, Guizhou, Hunan, Chongqing, and Sichuan. In 2010–2014, 111 high-high cluster counties were distributed across Guangxi, Guangdong, Hunan, Guizhou, Hainan, Jiangsu, Chongqing, and Yunnan. The 2015–2019 period revealed 59 high-high cluster counties spanning Hunan, Guangxi, Guangdong, Chongqing, Sichuan, Guizhou, Henan, Hubei, Jiangsu, Anhui, Shandong, and Yunnan. Most recently, during 2020–2024, 32 high-high cluster counties were concentrated in Hunan, Henan,

Guangxi, Anhui, and Hubei. The number of high-high cluster counties declined progressively throughout the study period. Notably, while the absolute number of cluster counties decreased, the geographic distribution of affected PLADs initially broadened from 2005 through 2019, incorporating additional central and eastern PLADs, before subsequently contracting to a more focused regional pattern after 2019 (Table 2).

Spatiotemporal Clustering Analysis

Retrospective spatiotemporal scan analysis identified seven statistically significant rabies transmission clusters: one primary cluster and six secondary clusters (Table 3). The primary cluster occurred from September to November 2006, spanning the border regions of Guangxi, Hunan, Guizhou, and Guangdong PLADs. Six secondary clusters emerged sequentially across different geographic areas and time periods: August-October 2006 (Henan, Anhui, Hubei, and adjacent PLADs); August-October 2007 (Sichuan-Chongqing-Shaanxi-Hubei border July-September 2007 (Hebei-Shandong-Tianjin); July-September 2010 (Yunnan Province exclusively); July-September 2011 (Shanxi-Shaanxi border); and December 2013–January 2014 (Shanxi-Inner Mongolia-Hebei-Shaanxi).

These clusters demonstrated distinct spatiotemporal aggregation patterns. Five of the seven clusters exhibited marked seasonal concentration during late summer and early autumn (July–October). Geographically, transmission showed a pronounced preference for interprovincial border zones, with the primary cluster and five secondary clusters positioned

TABLE 1. Distribution of human rabies cases in China, 2023–2024.

PLADs	Reported cases (n)			Number of counties reporting cases (n)			
PLADS	2023	2024	Increased	2023	2024	Increased	
Henan	35	49	14	26	27	1	
Guangxi	11	22	11	10	15	5	
Jiangsu	5	12	7	5	10	5	
Hubei	6	13	7	6	9	3	
Guizhou	3	9	6	3	8	5	
Hunan	16	19	3	13	16	3	
Anhui	9	12	3	8	9	1	
Shanxi	2	5	3	1	4	3	
Hebei	1	3	2	1	3	2	
Shanghai	0	1	1	0	1	1	
Fujian	0	1	1	0	1	1	
Hainan	0	1	1	0	1	1	
Sichuan	4	4	0	4	4	0	
Zhejiang	3	3	0	3	3	0	
Shandong	3	3	0	3	2	-1	
Yunnan	2	1	-1	2	1	-1	
Jiangxi	7	5	-2	7	4	-3	
Chongqing	4	1	-3	3	1	-2	
Guangdong	6	2	-4	5	2	-3	
Shaanxi	5	1	-4	2	1	-1	
Total	122	167	45	102	122	20	

Abbreviation: PLADs=provincial-level administrative divisions.

TABLE 2. Spatial autocorrelation analysis of rabies cases in China (County level), 2005–2024.

Time -	Global spatial autocorrelation		Local spatial autocorrelation				
Time	Moran's I	P	High-high clusters	High-low clusters	Low-high clusters	Low-low clusters	
2005–2009	0.519	<0.05	130	0	31	27	
2010–2014	0.431	<0.05	111	3	41	25	
2015–2019	0.294	<0.05	59	4	28	52	
2020–2024	0.331	<0.05	32	3	10	58	

TABLE 3. Retrospective space-time scan analysis of rabies cases in China, 2005–2024.

Cluster type	n	Location PLADs	Time	Observed/Expected
Primary cluster	291	Guangxi (108), Hunan (74), Guizhou (69),	September 1, 2006 to November 30, 2006	477.0/37.6
Secondary cluster-1		Guangdong (37), Chongqing (2), Yunnan (1) Sichuan (90), Chongqing (34), Shaanxi (24), Hubei (4), Gansu (3)	August 1, 2007 to October 31, 2007	(Ratio: 12.68) 182.0/27.7 (Ratio: 6.56)
Secondary cluster-2	549	Henan (143), Anhui (93), Hubei (91),	August 1, 2006 to October 31, 2006	297.0/97.9 (Ratio: 3.03)
Secondary cluster-3	41	Shanxi (23), Shaanxi (16), Hunan (2)	July 1, 2011 to September 30, 2011	38.0/4.3 (Ratio: 8.74)
Secondary cluster-4	102	Hebei (77), Shandong (16), Tianjin (9)	July 1, 2007 to September 30, 2007	64.0/14.2 (Ratio: 4.50)
Secondary cluster-5	67	Shanxi (61), Shaanxi (3), Inner Mongolia (2), Hebei (1)	December 1, 2013 to January 31, 2014	29.0/3.6 (Ratio: 8.06)
Secondary cluster-6	81	Yunnan (81)	July 1, 2010 to September 30, 2010	39.0/8.1 (Ratio: 4.83)

Abbreviation: PLADs=provincial-level administrative divisions.

at multi-PLAD junctions. Temporally, outbreaks manifested across different years (2006, 2007, 2010, 2011, 2013–2014) without recurring annually in identical locations, indicating dynamically shifting epidemic foci. The analysis also revealed substantial variation in outbreak scale, exemplified by the geographically confined, single-province cluster in Yunnan (2010). Notably, the December 2013–January 2014 cluster represented an atypical winter occurrence, deviating from the predominant summer-autumn pattern.

In summary, rabies transmission exhibited spatiotemporal clustering characterized predominantly by summer-autumn peaks concentrated in interprovincial border regions. This pattern was accompanied by additional complexities, including interannual variation in outbreak timing and location, geographically localized transmission events, and occasional atypical seasonal occurrences.

Spatial Occurrence Frequency Analysis

We conducted spatial frequency analysis at the county level to identify areas with persistent rabies transmission throughout the study period. Between 2005 and 2024, we identified 352 high-frequency counties (defined as reporting cases in ≥10 years over 20-year period) in China, predominantly concentrated in central and southern regions. The five PLADs with the greatest number of high-frequency counties were Guangxi (53 counties), Hunan (39 counties), Guizhou (35 counties), Guangdong (33 counties), and Henan (32 counties) (Table 4). Individual counties demonstrating the highest case frequencies included Sheqi County in Henan Province (20 cases), Dongxing City in Guangxi (19 cases), Zixing City in Hunan (19 cases), Dongkou County in Hunan (18 cases), and Shangcheng County in Henan (18 cases).

Demographic Characteristics of Human Rabies Cases

Between 2005 and 2024, reported human rabies cases in China ranged from neonates (less than 1 month old) to elderly individuals aged 96 years. Age distribution analysis demonstrated that the 41–70 year age group accounted for the highest proportion of cases (53.8%), followed by individuals aged 6–20 years (14.9%). Gender analysis revealed 17,317 male cases and 7,429 female cases, corresponding to a male-to-female ratio of 2.3:1. Occupational stratification

TABLE 4. Occurrence frequency of human rabies in China, 2005–2024.

PLADs	Number of high-frequency districts/counties (n)
Guangxi	53
Hunan	39
Guizhou	35
Guangdong	33
Henan	32
Hubei	23
Jiangsu	22
Sichuan	19
Anhui	19
Shandong	14
Yunnan	12
Jiangxi	12
Chongqing	11
Zhejiang	9
Hebei	5
Shanxi	4
Hainan	3
Shaanxi	2
Inner Mongolia	2
Shanghai	1
Heilongjiang	1
Fujian	1
Total	352

Abbreviation: PLADs=provincial-level administrative divisions.

identified farmers as the most heavily affected group, representing 68.6% of all cases, while students and children constituted the second-largest demographic category (Table 5).

CONCLUSIONS

From 2005 to 2024, China's rabies epidemic demonstrated a biphasic trajectory characterized by an initial peak in 2007, followed by 16 consecutive years of decline through 2023, and a subsequent resurgence in 2024. Despite this recent increase, 2024 case numbers remained substantially lower than those recorded during 2005-2019. This sustained reduction demonstrates effectiveness of the China's comprehensive prevention and control strategy implemented since 2006, which prioritized strengthening human rabies surveillance, conducting epidemic containment and source elimination, and enhancing dog management and vaccination (5).

TABLE 5. Demographic characteristics of human rabies cases in China, 2005–2024.

Group division	Human rabies cases (n)	Proportion (%)	
Gender			
Male	17,317	70.0	
Female	7,429	30.0	
Age (years)			
0–5	1,503	6.1	
6–20	3,684	14.9	
21–40	3,426	13.8	
41–70	13,302	53.8	
71 and older	2,831	11.4	
Occupation			
Farmer	16,983	68.6	
Student	3,004	12.1	
Children living at home	1,617	6.5	
Unemployed	780	3.2	
Other	2,362	9.6	

Analysis of 2024 cases revealed that only 4.1% of affected counties (5 counties, 6 cases) reported their first cases in two decades, whereas 95.9% represented recurrences in historically endemic areas. This distribution pattern suggests that the recent increase represents localized resurgence within established hotspots rather than geographic expansion of transmission.

Spatial autocorrelation analysis demonstrated a distinct northward shift in China's rabies high-risk core areas over the past two decades. The most recent five-year period (2020–2024) showed concentration primarily in interprovincial border regions of Henan, Hunan, Guangxi, Hubei, and Anhui. Although annual case counts in all high-incidence PLADs have decreased significantly from peak levels, and spatiotemporal scanning detected no new disease clusters emerging after 2014, this geographic transition of high-risk zones principally reflects regional variations in the pace of epidemic decline. The current high-risk core areas represent regions where case reduction has progressed more slowly during the recent five-year period.

Spatial occurrence frequency analysis identified persistent high-incidence counties with consistent case detection throughout the 20-year surveillance period. These endemic hotspots were predominantly concentrated central and southern China, particularly Guangxi, Hunan, Guizhou,

Guangdong, Henan, Hubei, and Jiangsu — geographic distributions that aligned precisely with hotspot regions identified through spatial autocorrelation analysis. Notably, 50.8% of counties reporting more than one case in 2024 were these historically high-frequency zones. Despite China's overall transition to low sporadic transmission, these areas continue to face substantial challenges, including: 1) inadequate canine rabies control, 2) sustained high transmission risks, and 3) particular difficulties for elimination efforts. These counties, therefore, represent priority targets for intensified, tailored interventions.

Scattered high-frequency counties were identified historically low-incidence in **PLADs** including Hainan, Inner Mongolia, Shaanxi, Heilongjiang, Fujian, and Shanghai. This distribution suggests persistent viral circulation among reservoir animals in these regions. The low human case numbers in these areas may reflect effective post-exposure coverage protecting exposed prophylaxis (PEP) individuals, though further investigation is needed to confirm this hypothesis and identify other contributing factors.

Demographic analysis demonstrates that farmers continue to bear the greatest burden of human rabies in China, consistent with established research findings (9). This disproportionate vulnerability arises from interconnected challenges in rural settings, including inadequate canine population management with suboptimal vaccination coverage, limited community awareness of rabies prevention measures, insufficient uptake of PEP services (10). investigation identified geographically concentrated hotspots that persistently report elevated case numbers and frequencies despite overall declining trends in surrounding rural areas. These persistent transmission zones appear to reflect multiple contributing factors, including sustained rabies virus circulation among local dog populations, culturally rooted practices that increase human-animal contact, and structural barriers that limit timely access to PEP services due to either geographic availability or financial constraints. The persistence of these well-defined hotspots underscores the critical need for comprehensive field studies to elucidate the complex interplay of biological, behavioral, and health system factors that sustain rabies transmission in these specific localities.

This study documents China's epidemiological transition in human rabies from relatively widespread regional endemicity to a pattern of highly sporadic occurrence with localized clustering. The current risk

profile demonstrates concentrated transmission within previously identified High-High clusters, particularly in persistent high-incidence counties showing notable case resurgence — these areas represent critical intervention targets. These findings support the implementation of refined prevention strategies focused on high-risk areas through: comprehensive investigation of the root causes of persistent transmission; implementation of geographically tailored control measures using a "one-county-onepolicy" framework; and development of precision interventions that address distinct local risk factors. This approach recognizes the necessity of moving beyond uniform national strategies to address the evolving, heterogeneous nature of rabies distribution across China's diverse epidemiological landscape.

This study was subject to some limitations: Our reliance on human rabies surveillance data alone represents a significant limitation, as this approach cannot fully capture actual transmission risks without incorporating data from the critical animal reservoir component. A more comprehensive risk assessment would require an integrated analysis combining human case data with systematic animal rabies monitoring to accurately evaluate regional control progress and transmission dynamics. Future investigations should integrate data on canine vaccination coverage with the spatial and temporal incidence of canine rabies to provide a complete epidemiological picture. This integrated approach is essential for developing robust transmission dynamics models that can accurately identify and characterize transmission hotspots, thereby informing more effective control strategies.

Conflicts of interest: No conflicts of interest.

doi: 10.46234/ccdcw2025.227

Disease Control and Prevention (Chinese Academy of Preventive Medicine), Beijing, China; ³ Beijing Daxing District Center for Disease Control and Prevention, Beijing, China; ⁴ National Key Laboratory of Intelligent Tracking and Forecasting for Infectious Diseases, Chinese Center for Disease Control and Prevention (Chinese Academy of Preventive Medicine), Beijing, China.

Copyright © 2025 by Chinese Center for Disease Control and Prevention. All content is distributed under a Creative Commons Attribution Non Commercial License 4.0 (CC BY-NC).

Submitted: July 21, 2025 Accepted: October 16, 2025 Issued: October 24, 2025

REFERENCES

- Fooks AR, Banyard AC, Horton DL, Johnson N, McElhinney LM, Jackson AC. Current status of rabies and prospects for elimination. Lancet 2014;384(9951):1389 – 99. https://doi.org/10.1016/S0140-6736(13)62707-5.
- Hampson K, Coudeville H, Lembo T, Sambo M, Kieffer A, Attlan M, et al. Correction: estimating the global burden of endemic canine rabies. PLoS Negl Trop Dis 2015;9(5):e0003786. https://doi.org/10.1371/journal.pntd.0003786.
- Zhou H, Vong S, Liu K, Li Y, Mu D, Wang LP, et al. Human rabies in China, 1960-2014: a descriptive epidemiological study. PLoS Negl Trop Dis 2016;10(8):e0004874. https://doi.org/10.1371/journal.pntd. 0004874.
- Zhao LX, Xia Y, Kiesel A, Li YF, Liao CH, Lu JY, et al. Epidemiological trends of rabies and control strategy in China: a narrative review. One Health Bull 2023;3(1):1. https://doi.org/10. 4103/2773-0344.363563.
- Yin WW, Fu ZF, Gao GF. Progress and prospects of dogmediatedrabies elimination in China. China CDC Wkly 2021;3(39): 831 – 4 https://doi.org/10.46234/ccdcw2021.205.
- Chinese Center For Disease Control and Prevention. Guidelines for the Management of Rabies Exposure Prophylaxis and Guidelines for the Diagnosis and Treatment of Rabies. [EB/OL]. (2023-9-13)[2025-10-21]. https://www.chinacdc.cn/jkyj/crb2/yl/kqb/jswj_kqb/.
- 7. Qin Y, Zhang Q, Lai SJ, Chen QL, Ren Q, Yin WW, et al. Analysis of epidemic characteristics of human rabies in China in 2007-2023. Chin J Exp Clin Virol 2024;38(4):373 7. https://doi.org/10.3760/cma.j. cn112866-20240403-00055.
- 8. Yue YJ, Chen QL, Mu D, Li Y, Yin WW. A descriptive analysis of human rabies in mainland China, 2005-2020. Int J Environ Res Public Health 2022;20(1):380. https://doi.org/10.3390/ijerph20010380.
- 9. Liu ZR, Liu M, Tao XY, Zhu WY. Epidemic characteristics of human rabies China, 2016-2020. China CDC Wkly 2021;3(39):819 21. https://doi.org/10.46234/ccdcw2021.203.
- Zhang XM, Tian XY, Pang B, Wang ZQ, Zhai WJ, Jiang XL, et al. Epidemiological characteristics of human rabies — Shandong Province, China, 2010-2020. China CDC Wkly 2022;4(35):793 – 7. https://doi. org/10.46234/ccdcw2022.055.

^{*} Corresponding author: Di Mu, mudi@chinacdc.cn.

¹ National Key Laboratory of Intelligent Tracking and Forecasting for Infectious Diseases, National Institute for Communicable Disease Control and Prevention, Chinese Center for Disease Control and Prevention (Chinese Academy of Preventive Medicine), Beijing, China; ² China Field Epidemiology Training Program, Chinese Center for

Vital Surveillances

Genomic Characterization of Human Adenovirus Type 21 Strains — 7 PLADs, China, 2023–2024

Yali Jin¹; Naiying Mao¹; Xueping Ma²; Linqing Zhao³; Liwei Sun⁴; Jikui Deng⁵; Shu Liang⁶; Hongmei Xu⁻; Xin Li³; Chunyu Zhu¹; Baicheng Xia¹; Aili Cui¹; Yan Zhang¹; Zhen Zhu¹.♯

ABSTRACT

Introduction: Recent sentinel surveillance has revealed a rising prevalence of human adenovirus type 21 (HAdV-21) among HAdV infections in China. This study aimed to elucidate the molecular features of currently circulating HAdV-21 strains in China.

Methods: Whole-genome sequencing (WGS) was performed on 23 HAdV-21 strains isolated from acute respiratory infection cases, 56.5% involving lower respiratory tract infections, across 7 Chinese sentinel surveillance provincial-level administrative divisions (PLADs) (2023–2024). These sequences, along with 50 previously reported HAdV-21 genomes from 6 countries (1956–2019), were integrated into a WGS dataset for comprehensive phylogenetic, genetic variation, and recombination analyses.

Results: WGS categorized the HAdV-21 strains into 3 subtypes: HAdV-21a, HAdV-21b, and historical HAdV-21p (isolated in the 1950s). HAdV-21a (1956-2024, involving 5 of the 6 countries) and HAdV-21b (2005-2024, involving 3 of the 6 exhibited extensive spatiotemporal countries) distributions. Recent Chinese strains (2023-2024) belonged to HAdV-21a and HAdV-21b (HAdV-21a/b), showing extremely high genetic homology with Chinese 2019 strains (genetic distance: 0.00007) and global strains (distance: <0.00040). Phylogenetic analysis confirmed that HAdV-21a/b shared a common ancestor and maintained a highly conserved genome despite decades of circulation. Sequence variation analysis identified shared and subtype-specific mutations in these two subtypes. Recombination pattern analysis further revealed that HAdV-21a/b acquired an HAdV-3-derived fragment in the E4 region (breakpoint: nt32,843).

Conclusions: Recombinant HAdV-21a/b subtypes have co-circulated in China in recent years with remarkable genetic conservation. Enhanced surveillance is essential to quantify associated disease

burden and guide targeted prevention and control strategies.

Human adenoviruses (HAdVs) are non-enveloped, double-stranded DNA viruses (genome size 34–36 kb) in the genus *Mastadenovirus* (family *Adenoviridae*), classified into 7 species (A–G) with 116 recognized types (http://hadvwg.gmu.edu/) (1). Among these, HAdV-3, HAdV-7, HAdV-55, HAdV-4, and species C (HAdV-C) are the major epidemiologically significant causes of respiratory infections (2–6).

HAdV-21 (species B), first identified in Saudi Arabia in 1956, is increasingly recognized as a significant pathogen in military and civilian populations across multiple countries (7). Although a of Chinese surveillance meta-analysis (2009-2021) revealed a low prevalence of HAdV-21 (0.87%), recent data from 14 sentinel surveillance sites across 11 provincial-level administrative divisions (PLADs) (2023–2024) indicated a marked increase: the proportion of HAdV-21 infections rose from 1.44% (2/139) in 2023 to 8.97% (21/234) in 2024 (Fisher's exact test: P=0.003) (unpublished data) (6). However, molecular epidemiological data on HAdV-21 in China remain limited, with only 3 isolates reported before 2023 (8-9).

To investigate the potential genetic correlations among the increasingly detected HAdV-21, this study performed whole-genome sequencing (WGS) of 23 HAdV-21 strains isolated from acute respiratory infections across 7 surveillance PLADs (2023–2024) and conducted phylogenetic, genetic variation, and recombination analyses by integrating these data with previously reported HAdV-21 genomes obtained from GenBank.

METHODS

Between 2023 and 2024, 23 HAdV-21 strains were

isolated from 7 Chinese sentinel surveillance PLADs Jilin, Ningxia, Liaoning, Guangdong, Chongqing, and Beijing) and confirmed by real-time polymerase chain reaction and amplification/analysis of 3 genes (penton base, hexon, and fiber). The corresponding 23 clinical cases ranged from 5 months to 68 years (median: 3 years). Among these cases, 14 (60.87%) required hospitalization. Ten cases presented with upper respiratory tract infections, while the remaining 13 had lower respiratory tract infections, including 10 with pneumonia. Co-infections occurred in 13 cases, most commonly with Haemophilus influenzae (5/13). One fatal case (Ningxia2024-669) of respiratory syndrome exhibited distress Mycoplasma pneumoniae co-infection (Table 1).

Viral DNA from the 23 strains was extracted using the QIAamp DNA Mini Kit (Qiagen, Hilden, Germany). WGS was performed by iGeneTech Biotechnology Co., Ltd. using probe-based hybrid capture combined with next-generation sequencing. All strains achieved 100% genome coverage, each yielding >1 Gb of data at >8,000× depth. Suboptimal regions were validated by Sanger sequencing, and two strains were randomly resequenced for quality assurance. Genome annotation was performed in Geneious Prime (version 2023.2.2, Biomatters Ltd., Auckland, New Zealand) using the HAdV-21 prototype strain (AY601633) as a reference.

Fifty HAdV-21 genomes from 6 countries (1956–2019), including 3 from China (2019) and 47 from other countries (1956–2018), were retrieved from GenBank (Supplementary Table S1, available at https://weekly.chinacdc.cn/). Integration of the 23 newly sequenced strains yielded a comprehensive

TABLE 1. Detailed information on the 23 HAdV-21 strains analyzed in this study.

Strain	PLADs	Gender	Age	Case type	Year of collection	Co-infection pathogens	Clinical diagnosis	Subtype
Jilin2023-296	Jilin	Female	3 years	Inpatient	2023/5/21	1	Bronchopneumonia	HAdV-21a
Jilin2023-595	Jilin	Female	3 years	Inpatient	2023/6/19	1	Upper respiratory infection	HAdV-21a
Ningxia2024-533	Ningxia	Male	3 years	Outpatient	2024/2/10	SARS-CoV-2	Fever	HAdV-21a
Ningxia2024-595	Ningxia	Female	5 months	Inpatient	2024/3/4	Hi	Severe lung infection/Lung consolidation	HAdV-21a
Ningxia2024-608	Ningxia	Female	5 years	Outpatient	2024/3/1	MP	Acute tonsillitis	HAdV-21a
Ningxia2024-618	Ningxia	Male	13 years	Outpatient	2024/3/5	Hi	Upper respiratory infection	HAdV-21a
Ningxia2024-669*	Ningxia	Male	9 months	Inpatient	2024/3/14	MP	Severe lung infection/ARDS	HAdV-21a
Ningxia2024-671	Ningxia	Female	5 years	Inpatient	2024/3/18	1	Severe lung infection/Lung consolidation	HAdV-21a
Ningxia2024-725	Ningxia	Male	13 years	Outpatient	2024/3/27	MP/Flu B	Respiratory infection	HAdV-21a
Ningxia2024-747	Ningxia	Male	6 years	Inpatient	2024/4/1	MP	Lung infection/Acute suppurative tonsillitis	HAdV-21a
Ningxia2024-754	Ningxia	Female	3 years	Outpatient	2024/3/31	Hi	Acute bronchitis	HAdV-21a
Ningxia2024-868	Ningxia	Female	4 years	Outpatient	2024/4/29	SP/Hi	Respiratory infection	HAdV-21a
Ningxia2024-907	Ningxia	Female	7 months	Outpatient	2024/5/8	Hi	Respiratory infection	HAdV-21a
Ningxia2024-944	Ningxia	Male	2 years	Outpatient	2024/5/21	SP	Fever	HAdV-21a
Beijing2024-330	Beijing	Female	3 years	Inpatient	2024/3/28	HRV	Bronchopneumonia	HAdV-21a
Beijing2024-364	Beijing	Male	1 year	Inpatient	2024/5/6	1	Pneumonia	HAdV-21a
Beijing2024-378	Beijing	Male	2 years	Inpatient	2024/5/21	Flu B	Fever	HAdV-21a
Shenzhen2024-077	Guangdong	Male	8 months	Inpatient	2024/4/27	1	Pneumonia	HAdV-21a
Chongqing2024-069	Chongqing	Female	2 years	Inpatient	2024/4/2	1	Febrile convulsions/Bronchitis	HAdV-21a
Shenyang2024-163	Liaoning	Male	57 years	Outpatient	2024/3/12	1	Respiratory infection	HAdV-21a
Gansu2024-215	Gansu	Male	68 years	Inpatient	2024/2/17	1	Community-acquired pneumonia	HAdV-21a
Ningxia2024-674	Ningxia	Male	1 year	Inpatient	2024/3/18	1	Severe lung infection	HAdV-21b
Shenzhen2024-201	Guangdong	Male	3 years	Inpatient	2024/6/11	1	Acute laryngotracheobronchitis	HAdV-21b

^{*} Indicates fatalities.

Abbreviation: ARDS=acute respiratory distress syndrome; PLAD=provincial-level administrative division; Hi=*Haemophilus influenzae*; MP=*Mycoplasma pneumoniae*; Flu B=Influenza B virus; SP=*Streptococcus pneumoniae*.

Note: / means no co-infecting pathogens detected.

database of 73 WGSs for phylogenetic and genetic variation analyses.

Sequences were aligned using ClustalW, and sequence similarity was assessed using BioEdit. A maximum likelihood phylogenetic tree was constructed using MEGA Version 7.0, with bootstrap support values (>80%) indicated at the tree nodes. Genetic mutations were identified using Snipit (https://github.com/aineniamh/snipit), focusing on variations with frequencies >80%. Recombination was analyzed using SimPlot (window size: 1,000 bp; step size: 100 bp) and Recombination Detection Program v4 (RDP4).

RESULTS

Genomic Characterization

All 23 HAdV-21 strains were fully assembled (genome sizes: 35,364-35,393 bp; GC: approximately 51.2%), consistent with previous reports (8–9). Annotation using the HAdV-21 prototype strain as a reference identified 48 conserved protein-coding regions (Supplementary Table S2, available at https:// weekly.chinacdc.cn/). Sequence identity analysis among the 23 HAdV-21 strains was ≥99.7%. Strains with identical sequences were detected across different PLADs and years, e.g., the 2023 Jilin strains (Jilin2023-296 and Jilin2023-595) matched 2024 strains from 5 PLADs (Beijing2024-364, Gansu2024-215, Ningxia2024-907, Shenyang2024-163, Shenzhen2024-077). Identical sequences were also detected within the same PLAD, such as Ningxia2024-595 and Ningxia2024-725.

The strains shared 98.8% nucleotide identity with the HAdV-21 prototype strain. Analysis of 12 functional domains, including major capsid proteins (penton base, hexon, fiber), core proteins (pV, pVII, pTP, pIVa2), minor proteins (pIX, pIIIa, pVI, pVIII), and the non-structural protein pX, showed relatively high similarity (nt: 98.4%–99.8%, aa: 97.9%–100.0%) across 11 regions, with the penton base showing lower conservation (nt: 96.3%, aa: 95.7%–95.9%).

Phylogenetic Analysis

To determine the genetic relationships between the 23 HAdV-21 strains (2023–2024) and previously circulating Chinese and globally prevalent strains, a phylogenetic analysis was performed using the constructed WGS dataset (Figure 1). The results showed that the 73 HAdV-21 strains were categorized

into 3 distinct evolutionary lineages: HAdV-21a, HAdV-21b, and HAdV-21p (bootstrap support >80%). HAdV-21a and HAdV-21b (HAdV-21a/b) exhibited closer phylogenetic relationships to each other (genetic distance=0.001) than to HAdV-21p (genetic distance=0.007 for both subtypes), indicating a shared ancestry for HAdV-21a/b.

Further analyses revealed distinct temporal and geographical distribution patterns among the 3 HAdV-21 subtypes. HAdV-21p primarily comprised a prototype strain from Saudi Arabia and a historical strain from Germany (1950s). Conversely, HAdV-21a comprised 21 strains from 7 Chinese PLADs (2023–2024), 3 Chinese strains from 2 PLADs (2019), and 24 strains from the United States, Malaysia, Germany, and Switzerland (1956-2016). HAdV-21b included 2 strains from 2 Chinese PLADs (2024) and 21 strains from the United States and Germany (2005-2018). All 3 subtypes demonstrated minimal intra-subtype variation (distance: genetic 0.00014-0.00031). HAdV-21a/b demonstrated high genetic consistency between 2023-2024 Chinese strains and both the 2019 Chinese strains (distance: 0.00007) and global strains (distance <0.00040), strongly suggesting close genetic relationships. No significant correlation was observed between clinical severity and 2 subtypes (HAdV-21a and HAdV-21b).

Genetic Variation

Genetic variation analysis of HAdV-21a/b was performed using WGS with the HAdV-21p prototype strain as a reference. The results showed that the 2 subtypes shared 352 specific nucleotide variants, including 64 insertions and 49 deletions, with HAdV-21a exhibiting 27 unique variants (10 deletions) and HAdV-21b displaying 36 unique variants (3 insertions and 18 deletions). The variants were distributed across the genome, with insertions and deletions concentrated in the L2 (46.90%) and E3 (23.01%) regions, respectively. Non-coding region variants were also detected in the Chinese HAdV-21a (4 sites, 1 insertion) and HAdV-21b (7 sites).

Amino acid variation analysis across the 12 functional domains identified 70 shared HAdV-21a/b substitutions in 11 proteins, excluding pX (Figure 2). 9 of 10 shared hexon gene variants were localized to hypervariable regions (HVRs), with HVR7 exhibiting the highest mutation frequency (4 sites). In the fiber gene, 2 of 3 variants occurred in the shaft region and one in the knob region. The penton base gene exhibited 23 variations, primarily clustered within the

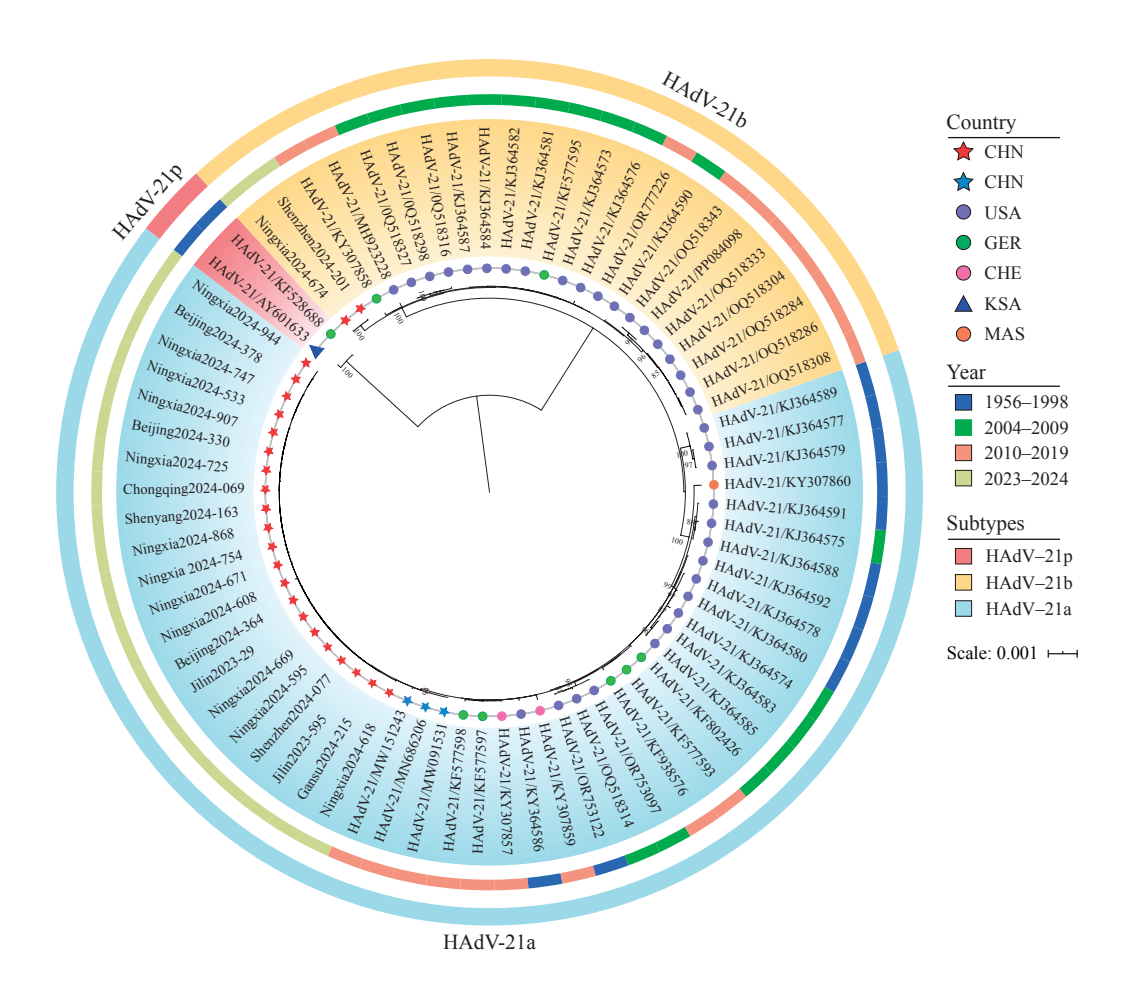


FIGURE 1. Maximum-likelihood phylogenetic trees of HAdV-21 were constructed from a dataset of 73 strains (23 from this study and 50 from the GenBank database). Trees derived from nine individual gene fragments of HAdV-21 are presented in panels A-I, and the tree based on the WGS is presented in panel J. The HAdV-21 and HAdV-3 prototype strains are marked in red and dark blue, respectively, across all panels

Abbreviation: WGS=whole-genome sequencing; HAdV-21=human adenovirus type 21.

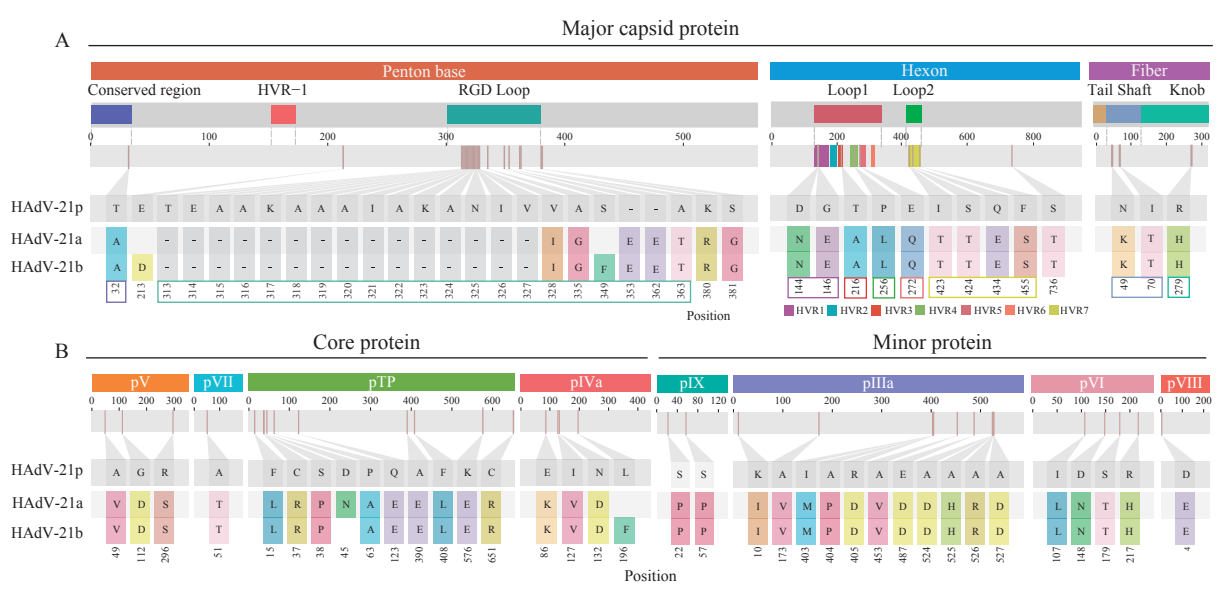


FIGURE 2. Amino acid variations in 11 key proteins of (A) HAdV-21a and (B) HAdV-21b subtypes compared to the prototype HAdV-21 strain (designated HAdV-21p). Abbreviation: HAdV-21=human adenovirus type 21.

RGD loop, including 15 amino acid deletions (313TEAAKAAAIAKANIV327) and 2 insertions (362EE363). Subtype-specific mutations were also detected, including pIVa2 (HAdV-21b: L196F), pTP (HAdV-21a: D45N), and penton base (HAdV-21b: E213D and S349F).

Genetic Recombination

To assess recombination, phylogenetic analysis was performed with the HAdV-21 strains and 18 species B prototype strains (Supplementary Table S1) using 9 consecutive genomic fragments (nt1-7,000;nt7,001–13,877; penton base; nt15,564–18,453; hexon; nt21,304-26,000; nt26,001-31,405; fiber; nt32,378-end) and WGS (Supplementary Figure S1, available at https://weekly.chinacdc.cn/). The results demonstrated that subtype classification using the nt32,378-end fragment matched the WGS-based classification, whereas the other 8 fragments failed to distinguish HAdV-21a/b. In the nt32,378-end region, HAdV-21a/b exhibited closer phylogenetic relationships with the HAdV-3 prototype strain, suggesting potential recombination in the E4 region. SimPlot and RDP4 analyses (supported by four

algorithms) further confirmed identical recombination patterns in both subtypes, with a breakpoint at nt32,843 in the E4 gene (Figure 3).

DISCUSSION

This study analyzed 23 HAdV-21 strains (2023–2024) isolated from patients with acute respiratory infections. Among these, 56.5% (13/23) had lower respiratory tract infections, including 9 pneumonia cases and 1 fatal infant case. To elucidate the genetic basis of these emerging strains, this study performed a comprehensive genomic characterization.

Phylogenetic analyses identified viral genetic subtypes and spatiotemporal transmission patterns. Globally, HAdV-21 strains are classified into 3 subtypes: HAdV-21a, HAdV-21b, and HAdV-21p. HAdV-21p, comprising historical strains from the 1950s, is no longer detected. Conversely, HAdV-21a (1956–2024, 5 countries) and HAdV-21b (2005–2024, 3 countries) demonstrated extensive spatiotemporal distribution, reflecting stable epidemic trends and highlighting these strains as the dominant circulating subtypes in multiple countries, including

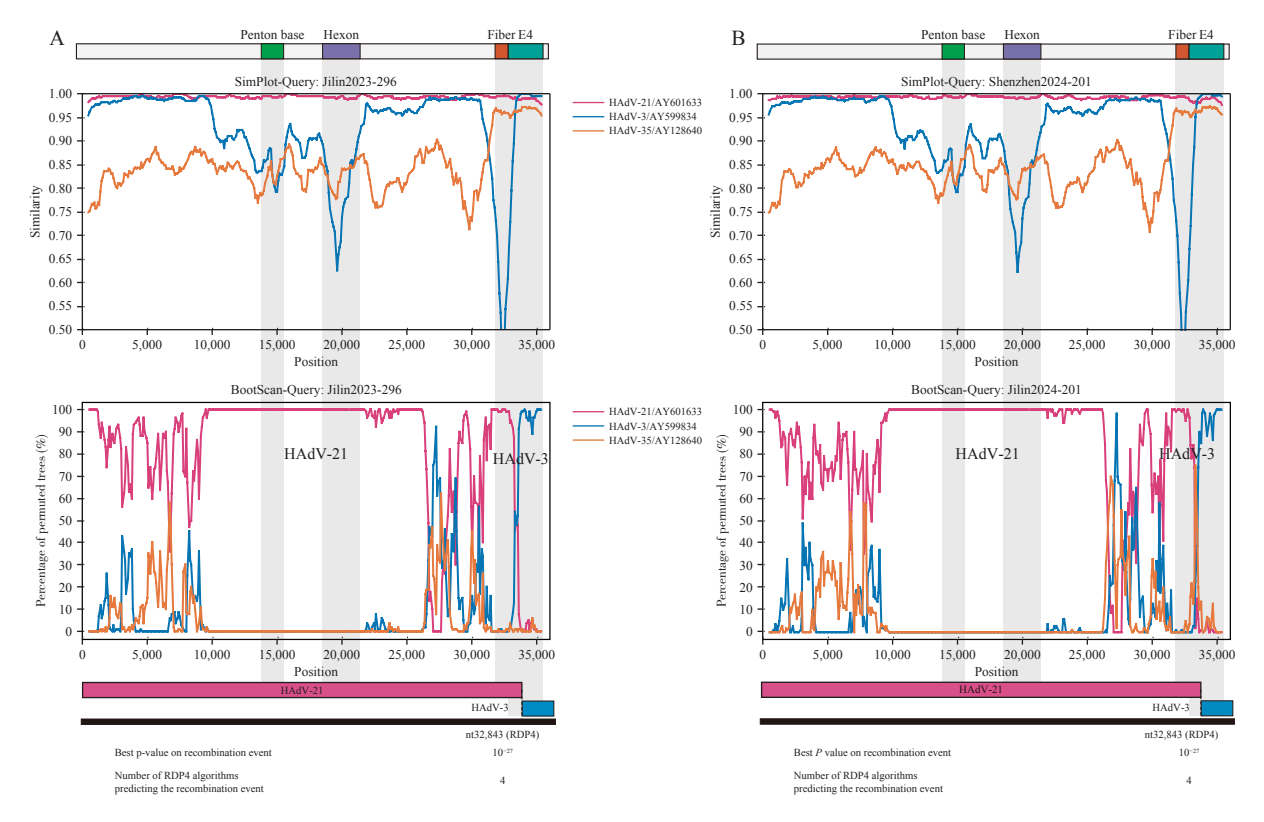


FIGURE 3. Recombinant analysis of (A) HAdV-21a and (B) HAdV-21b strains. Note: Jilin2023-296 and Shenzhen2024-201 were used as representative HAdV-21a and HAdV-21b strains, respectively. Abbreviation: HAdV-21=human adenovirus type 21.

China. Furthermore, all subtypes exhibited minimal intra-subtype genetic variation (distance <0.00031), suggesting genomic stability during prolonged circulation, consistent with observations in other HAdV types, such as HAdV-4 and HAdV-55 (10–11). This stability may result from the conserved replication mechanism of HAdV or selective equilibrium under host immune pressure.

Notably, Chinese HAdV-21a/b strains (2023-2024) exhibited extremely high genetic homology and consistency with 2019 Chinese strains (distance: 0.00007) and historical global strains (distance: <0.0040), indicating that the currently circulating HAdV-21 is not a novel variant but a continuous transmission of genetically related strains. Enhanced respiratory infection surveillance following coronavirus disease 2019 (COVID-19) likely contributed to increased detection rates in recent years. Although HAdV-21 demonstrates relatively lower virulence and infectivity than other common types (e.g., HAdV-3, -7, -4, -55), it is associated with diverse clinical manifestations, including severe pneumonia, acute respiratory distress syndrome, acute flaccid paralysis, myocarditis, and fatal outcomes across age groups, necessitating urgent research on its pathogenic characteristics (8–9, 12–14).

Phylogenetic and recombination analyses confirmed a common ancestor for HAdV-21a/b. Despite high overall genome conservation, sequence variation analysis identified both shared and subtype-specific mutations in HAdV-21a/b, representing key molecular markers for subtype differentiation and indicating continuous adaptive evolutionary pressure. Mutations in the hexon gene are predominantly localized in HVRs containing critical neutralizing antibody epitopes, suggesting that HVRs are primary adaptive targets for immune evasion. Consistent with previous studies, HAdV-21a/b exhibited 15 amino acid deletions and 2 insertions in the RGD loop of the penton base gene compared to the prototype strain. This shortened RGD loop closely resembles those of HAdV-3 and HAdV-7, which are associated with severe diseases (15). Because the RGD loop is a core functional domain mediating viral cell entry, its alteration may directly affect viral pathogenicity and efficiency; therefore, the functional consequences of the penton base warrant further investigation.

Recombination analysis revealed that HAdV-21a/b acquired an HAdV-3-derived fragment in the E4 region (breakpoint: nt32,843). As E4 regulates viral

DNA replication, transcript splicing, and late gene expression, this recombination likely enhances viral stability and replication efficiency through functional complementation, thereby conferring transmission advantages. Genetic recombination drives HAdV evolution, where adaptive recombination patterns establish stable transmission, as exemplified by HAdV-21a and HAdV-21b persisting in circulation for approximately 70 and 20 years, respectively.

The findings in this report are subject to at least three limitations. First, HAdV-21 strains were collected from only 7 Chinese PLADs, limiting the generalizability of the findings; broader sampling in future work would improve representativeness. Second, the impact of HAdV-21 genomic differences on viral infection phenotypes remains unclear, warranting further investigation. Finally, although this study identified a significant HAdV-3 fragment-containing recombination event, functional validation was lacking, necessitating additional experiments to clarify its implications for viral pathogenicity and transmission.

In conclusion, this study identified the cocirculation of HAdV-21a and HAdV-21b in China and characterized their genomic features. Given HAdV-21's increasing prevalence, persistence of similar viruses across multiple PLADs, and potential association with severe clinical outcomes, enhanced surveillance is required to quantify disease burden in China and provide targeted prevention and control strategies.

Conflicts of interest: No conflicts of interest.

Acknowledgements: The study used only viral strains and did not involve specimen collection. We sincerely thank the seven sentinel surveillance PLADs for providing the viral strains and associated data.

Funding: Supported by the National Key R&D Program of China (2022YFC2305303) and the Health and Wellness Sector Research Program of Gansu (GSWSON2021-010).

doi: 10.46234/ccdcw2025.228

^{*} Corresponding author: Zhen Zhu, zhuzhen@ivdc.chinacdc.cn.

¹ National Key Laboratory of Intelligent Tracking and Forecasting for Infectious Disease, NHC Key Laboratory of Medical Virology and Viral Diseases, National Institute for Viral Disease Control and Prevention, Chinese Center for Disease Control and Prevention, Beijing, China; ² Testing and Inspection Institute, Ningxia Hui Autonomous Region Center for Disease Control and Prevention, Yinchuan City, Ningxia Hui Autonomous Region, China; ³ Laboratory of Virology, Beijing Key Laboratory of Etiology of Viral Diseases in Children, Capital Institute of Pediatrics, Beijing, China; ⁴ Precision Medicine Research Center, Children's Hospital of Changchun, Changchun City, Jilin Province, China; ⁵ Division of Infectious Diseases, Shenzhen Children's Hospital, Shenzhen City, Guangdong

Province, China; ⁶ Key Laboratory of Infectious Diseases of Gansu Province, Gansu Provincial Center for Disease Control and Prevention, Lanzhou City, Gansu Province, China; ⁷ Department of Infectious Diseases, Children's Hospital Affiliated to Chongqing Medical University, Chongqing, China; ⁸ Health Supervision Institute, Shenyang Center for Disease Control and Prevention, Shenyang City, Liaoning Province, China.

Copyright © 2025 by Chinese Center for Disease Control and Prevention. All content is distributed under a Creative Commons Attribution Non Commercial License 4.0 (CC BY-NC).

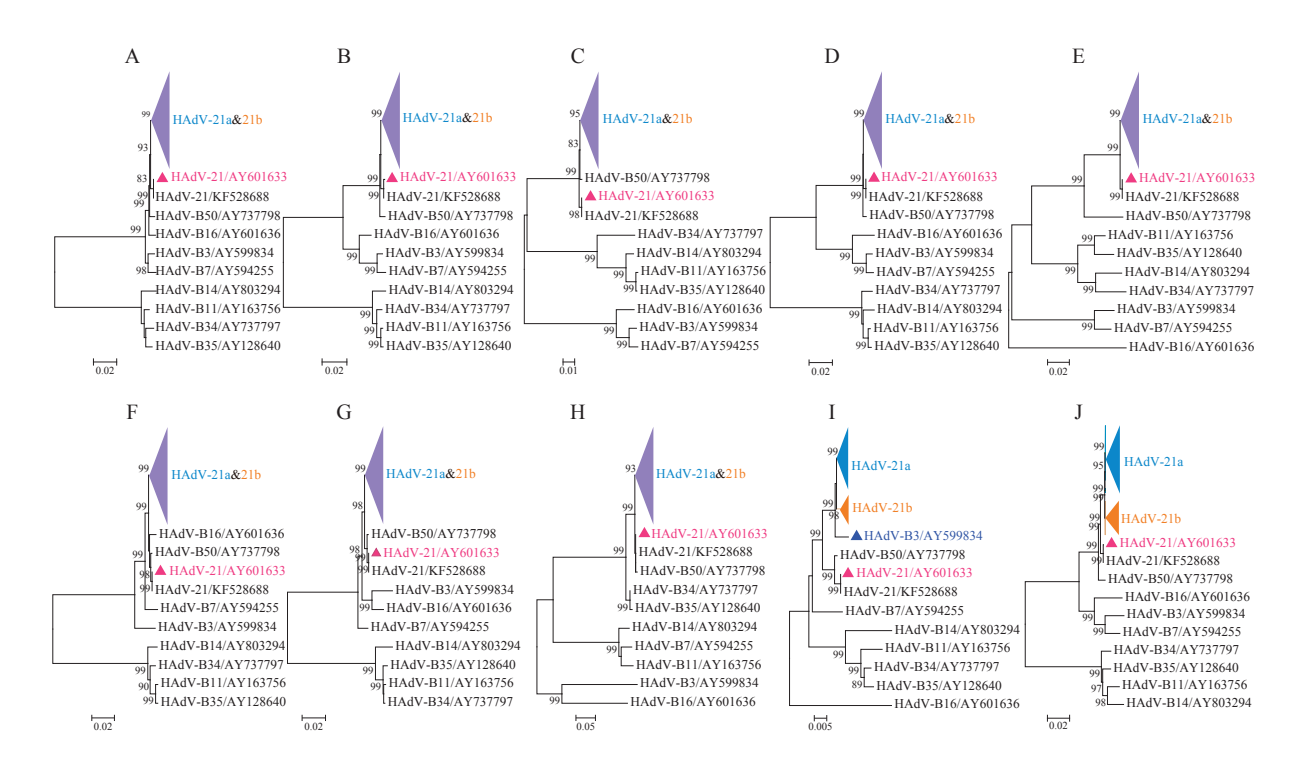
Submitted: July 02, 2025 Accepted: October 14, 2025 Issued: October 24, 2025

REFERENCES

- Davison AJ, Benkő M, Harrach B. Genetic content and evolution of adenoviruses. J Gen Virol 2003;84(Pt 11):2895-908. http://dx.doi.org/ 10.1099/vir.0.19497-0.
- Dou HX, Chen CM, Song TY, Sun X, He FF, Jia YJ, et al. Epidemiological characteristics and genomic analysis of respiratory adenovirus in Jining City from February 2023 to July 2024. BMC Genomics 2025;26(1):369. https://doi.org/10.1186/s12864-025-11558-1.
- 3. Wu CC, Zhang YF, Liang A, Wu XX, Zhu YQ, Huang ZX, et al. Comparative analysis between genotypes of adenovirus isolates from hospitalized children with acute respiratory tract infections and clinical manifestations in Wuhan, China, from June 2022 to September 2023. Virol Sin 2025;40(1):50 60. https://doi.org/10.1016/j.virs.2024.12.
- Mahmood K, Ahmed W, Farooq S, Habib G, Sindhu MA, Asif A, et al. Molecular characterization of human adenoviruses associated with pediatric respiratory infections in Karachi, Pakistan. BMC Infect Dis 2024;24(1):538. https://doi.org/10.1186/s12879-024-09415-9.
- Abbasi S, Shafiei-Jandaghi NZ, Shadab A, Hassani SA, Rahimi Foroushani A, Hosseinkhan N, et al. Phylogenetic characterization of rhinovirus and adenovirus in hospitalized children aged ≤ 18 years with severe acute respiratory infection in Iran. Iran J Microbiol 2023;15(1): 155 – 62. https://doi.org/10.18502/ijm.v15i1.11932.

- Liu MC, Xu Q, Li TT, Wang T, Jiang BG, Lv CL, et al. Prevalence of human infection with respiratory adenovirus in China: a systematic review and meta-analysis. PLoS Negl Trop Dis 2023;17(2):e0011151. https://doi.org/10.1371/journal.pntd.0011151.
- Bell SDJr, McComb DE, Murray ES, Chang RS, Snyder JC. Adenoviruses isolated from Saudi Arabia. I. Epidemiologic features. Am J Trop Med Hyg 1959;8(4):492 – 500. https://doi.org/10.4269/ajtmh. 1959.8.492.
- Ye FQ, Han YF, Zhu JJ, Li P, Zhang Q, Lin YF, et al. First identification of human adenovirus subtype 21a in China with MinION and illumina sequencers. Front Genet 2020;11:285. https:// doi.org/10.3389/fgene.2020.00285.
- Liu WK, Zhang L, Cai Y, Zhang Q, Chen DH, Qiu SY, et al. Human adenovirus subtype 21a isolates from children with severe lower respiratory illness in China. Front Microbiol 2022;13:924172. https:// doi.org/10.3389/fmicb.2022.924172.
- Wang JJ, Feng QY, Duan YL, Ai JH, Zhu Y, Wang R, et al. Human adenovirus type 4 (HAdV-4) associated acute respiratory tract infection in children & genetic characteristics of HAdV-4 in China: a prospective multicenter study. BMC Infect Dis 2024;24(1):936. https://doi.org/10. 1186/s12879-024-09835-7.
- Hang J, Kajon AE, Graf PCF, Berry IM, Yang Y, Sanborn MA, et al. Human adenovirus type 55 distribution, regional persistence, and genetic variability. Emerg Infect Dis 2020;26(7):1497 – 505. https:// doi.org/10.3201/eid2607.191707.
- Jia XB, Wan LL, Xiao F, Huang XL, Zhou J, Wang Y, et al. Rapid and sensitive detection of human adenovirus types 3 and 7 using CRISPR-Cas12b coupled with multiple cross displacement amplification. Infect Med 2025;4(2):100181. https://doi.org/10.1016/j.imj.2025.100181.
- 13. Abd-Jamil J, Teoh BT, Hassan EH, Roslan N, Abubakar S. Molecular identification of adenovirus causing respiratory tract infection in pediatric patients at the University of Malaya Medical Center. BMC Pediatr 2010;10(1):46. https://doi.org/10.1186/1471-2431-10-46.
- Pfortmueller CA, Barbani MT, Schefold JC, Hage E, Heim A, Zimmerli S. Severe acute respiratory distress syndrome (ARDS) induced by human adenovirus B21: report on 2 cases and literature review. J Crit Care 2019;51:99 – 104. https://doi.org/10.1016/j.jcrc.2019.02. 019.
- Hage E, Huzly D, Ganzenmueller T, Beck R, Schulz TF, Heim A. A human adenovirus species B subtype 21a associated with severe pneumonia. J Infect 2014;69(5):490 – 9. https://doi.org/10.1016/j.jinf. 2014.06.015.

SUPPLEMENTARY MATERIAL



SUPPLEMENTARY FIGURE S1. Maximum-likelihood phylogenetic tree constructed with 23 HAdV-21 strains from this study and 50 HAdV-21 strains from the GenBank database based on (A–I) nine fragments and (J) whole-genome sequence (WGS). The HAdV-21 prototype strain is indicated in red and HAdV-3 prototype strain is indicated in dark blue. Abbreviation: WGS=whole-genome sequencing, HAdV-21=human adenovirus type 21.

SUPPLEMENTARY TABLE S1. List of 50 HAdV-21 strains and 17 prototype strains of species B from GenBank.

No.	Strain name	Country	Year	Accession No.	Type
1	AV-1645	KSA	1956	AY601633	HAdV-21p
2	Human adenovirus 21	GER	1950s	KF528688	HAdV-21p
3	HAdV-B21/USA/7K4/1956	USA	1956	OR753122	HAdV-21a
4	CDC RU8176	USA	1978	KJ364577	HAdV-21a
5	CDC V1375E	USA	1984	KJ364579	HAdV-21a
6	VRDL T87-0342	USA	1987	KJ364591	HAdV-21a
7	CDC V2148A	USA	1988	KJ364588	HAdV-21a
8	NHRC 5	USA	1996	KJ364578	HAdV-21a
9	VRDL T97-1745	USA	1997	KJ364589	HAdV-21a
10	VRDL T98-1269	USA	1998	KJ364592	HAdV-21a
11	NHRC 10030	USA	1998	KJ364586	HAdV-21a
12	NHRC 20007	USA	1998	KJ364580	HAdV-21a
13	NHRC 71139	USA	2004	KJ364583	HAdV-21a
14	NHRC 71252	USA	2005	KJ364585	HAdV-21a
15	NHRC 32493	USA	2005	KJ364574	HAdV-21a
16	NHRC 63218	USA	2006	KJ364575	HAdV-21a
17	HAdV-B21/USA/5L10/2009	USA	2009	OR753097	HAdV-21a
18	HAdV-B21/USA/4B5/2009	USA	2009	OQ518314	HAdV-21a

China CDC Weekly

\sim			
Co	ntii	11 I I	חנ

No.	Strain name	Country	Year	Accession No.	Туре
19	Sibu-97	MAS	1997	KY307860	HAdV-21a
20	LRTI-2	GER	2008	KF802426	HAdV-21a
21	LRTI-3	GER	2010	KF577593	HAdV-21a
22	LRTI-4	GER	2012	KF938576	HAdV-21a
23	LRTI-5	GER	2012	KF577597	HAdV-21a
24	LRTI-6	GER	2013	KF577598	HAdV-21a
25	human/CHN/BB/201903/21	CHN	2019	MN686206	HAdV-21a
26	GZ06109.1	CHN	2019	MW091531	HAdV-21a
27	GZ09107.1	CHN	2019	MW151243	HAdV-21a
28	LRTI-7	CHE	2013	KY307857	HAdV-21a
29	LRTI-9	CHE	2016	KY307859	HAdV-21a
30	PEL0066	USA	2005	KJ364587	HAdV-21k
31	NHRC 71227	USA	2005	KJ364584	HAdV-21k
32	NHRC 32389	USA	2005	KJ364573	HAdV-21b
33	NHRC 52331	USA	2006	KJ364581	HAdV-21k
34	NHRC 44288	USA	2006	KJ364576	HAdV-21k
35	NHRC 91447	USA	2007	KJ364590	HAdV-21k
36	NHRC 64589	USA	2007	KJ364582	HAdV-21k
37	HAdV-B21/USA/2B2/2009	USA	2009	OQ518327	HAdV-21b
38	HAdV-B21/USA/2B10/2009	USA	2009	OQ518316	HAdV-21b
39	HAdV-B21/USA/4C7/2009	USA	2009	OQ518298	HAdV-21b
40	HAdV-B21/USA/6K2/2010	USA	2010	OQ518333	HAdV-21b
41	HAdV-B21/USA/9J5/2012	USA	2012	PP084098	HAdV-21b
42	HAdV-B21/USA/9I6/2012	USA	2012	OQ518343	HAdV-21k
43	HAdV-B21/USA/9M3/2012	USA	2012	OQ518308	HAdV-21b
44	HAdV-B21/USA/10E4/2012	USA	2012	OQ518304	HAdV-21b
45	HAdV-B21/USA/9M4/2012	USA	2012	OQ518286	HAdV-21b
46	HAdV-B21/USA/10E5/2012	USA	2012	OQ518284	HAdV-21b
47	HAdV-B21/USA/14A2/2017	USA	2017	OR777226	HAdV-21b
48	HAdVB/USA_NY/10208/2018/P21H21F21	USA	2018	MH923228	HAdV-21b
49	LRTI-1	GER	2005	KF577595	HAdV-21k
50	LRTI-8	GER	2016	KY307858	HAdV-21k
51	GB	USA	1953	AY599834	HAdV-B3
52	Gomen	USA	1954	AY594255	HAdV-B7
53	Ad11p Slobitski	USA	1957	AY163756	HAdV-B1
54	de Wit; ATCC VR-1091	NLD	1955	AY803294	HAdV-B14
55	ch. 79	USA	1955	AY601636	HAdV-B16
56	Compton; ATCC VR-716	USA	1972	AY737797	HAdV-B34
57	ATCC VR-718; Holden	USA	1973	AY128640	HAdV-B3
58	Wan; ATCC VR-1502	USA	1988	AY737798	HAdV-B50
59	QS-DLL	CHN	2006	FJ643676	HAdV-B5
60	87-922	ARG	1987	JN860676	HAdV-B66
61	Arg 827/04	ARG	2004	JN860678	HAdV-B68

No.	Strain name	Country	Year	Accession No.	Type
62	human/DEU/HEIM_00086/X/X[PXHXFX]	DEU	2013	KF633445	HAdV-B76
63	human/DEU/HEIM_00092/1985/NEW[P35H34F7]	DEU	1985	KF268328	HAdV-B77
64	HAdV-B/USA/CHOP2146-10810/2013/[P11H11F7]	USA	2013	KT970441	HAdV-B78
65	HAdV-B/JPN/T150125/2015/79[P11H34F11]	JPN	2015	LC177352	HAdV-B79
66	HAdV-B106[P11H11F35]	DEU	2020	ON393912	HAdV-B106
67	Human mastadenovirus B114	DEU	2023	OR853835	HAdV-B114

SUPPLEMENTARY TABLE S2-1. Genomic annotations of strains Jilin2023-296, Jilin2023-595, Ningxia2024-533, and Ningxia2024-595.

Gene	Encoded product	Jilin2023-296	Jilin2023-595	Ningxia2024-533	Ningxia2024-595
E1A	28.4 kDa protein 24.6 kDa protein	575–1,156; 1250–1,453 575–1,063; 1250–1,453	575–1,156; 1250–1,453 575–1,063; 1250–1,453	567–1,148; 1242–1,445 567–1,055; 1242–1,445	575–1,156; 1250–1,453 575–1,063; 1250–1,453
	6.8 kDa protein	575–646; 1,248–1,349	575–646; 1,248–1,349	567–638; 1,240–1,341	575–646; 1,248–1,349
E45	small T antigen	1,601–2,137	1,601–2,137	1,593–2,129	1,601–2,137
E1B	large T antigen (55K)	1,906-3,384	1,906–3,384	1,898–3,376	1,906–3,384
IX	hexon-associated protein IX	3,478-3,894	3,478-3,894	3,470–3,886	3,478–3,894
IVa2	maturation protein IVa2	3,947–5,280; 5,559–5,571	3,947–5,280; 5,559–5,571	3,939–5,272; 5,551–5,563	3,947–5,280; 5,559–5,571
	DNA polymerase	5,050–8,622; 13,841–13,849	5,050–8,622; 13,841–13,849	5,042–8,614; 13,834–13,842	5,050–8,622; 13,840–13,848
	hypothetical 11.5 kDa protein	6,143–6,463	6,143–6,463	6,135–6,455	6,143–6,463
	hypothetical 19 kDa protein	6,867–7,388	6,867–7,388	6,859–7,380	6,867–7,388
	hypothetical 10.4 kDa protein	7,132–7,419	7,132–7,419	7,124–7,411	7,132–7,419
E2B	DNA-binding protein	7,828–8,229; 9,479–9,496	7,828–8,229; 9,479–9,496	7,820–8,221; 9,471–9,488	7,828–8,622; 9,479–9,496
LZD	hypothetical 12.6 kDa protein	8,228-8,572	8,228-8,572	8,220-8,564	8,228-8,572
	terminal protein precursor	8,421–10,388; 13,841–13,849	8,421–10,388; 13,841–13,849	8,413–10,380; 13,834–13,842	8,421–10,388; 13,840–13,848
	hypothetical 14.5 kDa protein	8,547-8,948	8,547-8,948	8,539–8,940	8,547-8,948
	hypothetical 11.5 kDa protein	9,542–9,856	9,542–9,856	9,534–9,848	9,542–9,856
	hypothetical 9.7 kDa protein	9,756–10,031	9,756–10,031	9,748-10,023	9,756–10,031
L1	52 kDa protein	10,858–12,027	10,858–12,027	10,851–12,020	10,857–12,026
LI	protein IIIa precursor	12,055–13,818	12,055–13,818	12,048–13,811	12,054–13,817
	penton protein	13,891–15,540	13,891–15,540	13,884–15,533	13,890–15,539
	protein VII precursor	15,549–16,127	15,549–16,127	15,542–16,120	15,548–16,126
L2	protein V precursor	16,167–17,228	16,167–17,228	16,160–17,221	16,166–17,227
	protein X	17,257–17,487	17,257–17,487	17,250–17,480	17,256–17,486
	protein VI precursor	17,560–18,309	17,560–18,309	17,553–18,302	17,559–18,308
L3	hexon protein	18,423–21,272	18,423–21,272	18,416–21,265	18,422–21,271
	23 kDa proteinase	21,309–21,938	21,309–21,938	21,302–21,931	21,308–21,937
E2A	DNA-binding protein	22,027–23,580	22,027–23,580	22,020–23,573	22,026–23,579
	100 kDa hexon-assembly associated protein	23,611–26,094	23,611–26,094	23,604–26,087	23,610–26,093
	33 kDa protein	25,796–26,669	25,796–26,669	25,789–26,662	25,795–26,668
L4	22 kDa protein	25,796–26,395	25,796–26,395	25,789–26,388	25,795–26,394
	protein VIII	26,740–27,423	26,740–27,423	26,733–27,416	26,739–27,422

Gene	Encoded product	Jilin2023-296	Jilin2023-595	Ningxia2024-533	Ningxia2024-595
	12.1 kDa protein	27,423–27,743	27,423–27,743	27,416–27,736	27,422–27,742
	16 kDa protein	27,697–28,137	27,697–28,137	27,690–28,130	27,696–28,136
	19.2 kDa protein	28,122-28,640	28,122–28,640	28,115–28,633	28,121–28,639
	20 kDa protein	28,670-29,209	28,670–29,209	28,663–29,202	28,669–29,208
E3	21.2 kDa protein	29,222-29,834	29,222–29,834	29,215–29,827	29,221–29,833
	8.8 kDa protein	29,864–30,090	29,864-30,090	29,857-30,083	29,863-30,089
	10.3 kDa protein	30,130-30,405	30,130–30,405	30,123–30,398	30,129–30,404
	16.6 kDa protein	30,377–30,814	30,377–30,814	30,370-30,807	30,376–30,813
	15.3 kDa protein	30,807-31,214	30,807–31,214	30,800-31,207	30,806–31,213
L5	fiber protein	31,412–32,383	31,412–32,383	31,405–32,376	31,411–32,382
	16 kDa protein	32,415–32,666; 33,389–33,562	32,415–32,666; 33,389–33,562	32,408–32,659; 33,382–33,555	32,414–32,665; 33,388–33,561
E4	34.7 kDa protein	32,663–33,562	32,663–33,562	32,656–33,555	32,662–33,561
	14.3 kDa protein	33,465–33,833	33,465–33,833	33,458–33,826	33,464–33,832
L5	agnoprotein	33,688–34,197	33,688–34,197	33,681–34,190	33,687–34,196
	13.6 kDa protein	33,842–34,195	33,842–34,195	33,835–34,188	33,841–34,194
E4	14.4 kDa protein	34,192–34,581	34,192–34,581	34,185–34,574	34,191–34,580
	14.2 kDa protein	34,623-35,000	34,623-35,000	34,616–34,993	34,622-34,999

SUPPLEMENTARY TABLE S2-2. Genomic annotations of strains Ningxia2024-608, Ningxia2024-618, Ningxia2024-669, and Ningxia2024-671.

Gene	Encoded product	Ningxia2024-608	Ningxia2024-618	Ningxia2024-669	Ningxia2024-671
	28.4 kDa protein	575–11,56; 1,250–1,453	560–1,141; 1,235–1,438	575–1,156; 1250–1,453	575–1,156; 1,250–1,453
E1A	24.6 kDa protein	575–1,063; 1,250–1,453	560–1,048; 1,235–1,438	575–1,063; 1,250–1,453	575–1,063; 1,250–1,453
	6.8 kDa protein	575–646; 1,248–1,349	560–631; 1,233–1,334	575–646; 1,248–1,349	575–646; 1,248–1,349
E1B	small T antigen	1,601–2,137	1,586–2,122	1,601–2,137	1,601–2,137
LID	large T antigen (55K)	1,906–3,384	1,891–3,369	1,906–3,384	1,906–3,384
IX	hexon-associated protein IX	3,478-3,894	3,463–3,879	3,478-3,894	3,478–3,894
IVa2	maturation protein IVa2	3,947–5,280; 5,559–5,571	3,932–5,265; 5,544–5,556	3,947–5,280; 5,559–5,571	3,947–5,280; 5,559–5,571
	DNA polymerase	5,050–8,622; 13,840–13,848	5,035–8,607; 13,826–13,834	5,050–8,622; 13,841–13,849	5,050–8,622; 13,841–13,849
	hypothetical 11.5 kDa protein	6,143–6,463	6,128–6,448	6,143–6,463	6,143-6,463
	hypothetical 19 kDa protein	6,867–7,388	6,852-7,373	6,867–7,388	6,867–7,388
	hypothetical 10.4 kDa protein	7,132–7,419	7,117–7,404	7,132–7,419	7,132–7,419
E2B	DNA-binding protein	7,828–8,229; 9,479–9,496	7,813–8,214; 9,464–9,481	7,828–8,229; 9,479–9,496	7,828–8,229; 9,479–9,496
	hypothetical 12.6 kDa protein	8,228-8,572	8,213-8,557	8,228-8,572	8,228-8,572
	terminal protein precursor	8,421–10,388; 13,840–13,848	8,406–10,373; 13,826–13,834	8,421–10,388; 13,841–13,849	8,421–10,388; 13,841–13,849
	hypothetical 14.5 kDa protein	8,547-8,948	8,532-8,933	8,547-8,948	8,547-8,948
	hypothetical 11.5 kDa protein	9,542-9,856	9,527–9,841	9,542-9,856	9,542-9,856
	hypothetical 9.7 kDa protein	9,756–10,031	9,741–10,016	9,756–10,031	9,756–10,031
L1	52 kDa protein	10,857–12,026	10,843–12,012	10,858–12,027	10,858–12,027
LI	protein IIIa precursor	1,2054–1,3817	12,040-13,803	12,055–13,818	12,055–13,818

Gene	Encoded product	Ningxia2024-608	Ningxia2024-618	Ningxia2024-669	Ningxia2024-671
	penton protein	13,890–15,539	13,876–15,525	13,891–15,540	13,891–15,537
L2	protein VII precursor	15,548–16,126	15,534–16,112	15,549–16,127	15,551–16,129
LZ	protein V precursor	16,166–17,227	16,152–17,213	16,167–17,228	16,169–17,230
	protein X	17,256–1,7486	17,242–17,472	17,257–17,487	17,259–17,489
	protein VI precursor	17,559–18,308	17,545–18,294	17,560–18,309	17,562–18,311
L3	hexon protein	18,422–2,1271	18,408–21,257	18,423–21,272	18,425–21,274
	23 kDa proteinase	21,308–21,937	21,294–21,923	21,309–21,938	21,311–21,940
E2A	DNA-binding protein	22,026–23,579	22,012–23,565	22,027–23,580	22,029–23,582
	100 kDa hexon-assembly associated protein	23,610–26,093	23,596–26,079	23,611–26,094	23,613–26,096
1.4	33 kDa protein	25,795–26,668	25,781–26,654	25,796–26,669	25,798–26,671
L4	22 kDa protein	25,795–26,394	25,781–26,380	25,796–26,395	25,798–26,397
	protein VIII	26,739–27,422	26,725–27,408	26,740–27,423	26,742–27,425
	12.1 kDa protein	27,422–27,742	27,408–27,728	27,423–27,743	27,425–27,745
	16 kDa protein	27,696–28,136	27,682–28,122	27,697–28,137	27,699–28,139
	19.2 kDa protein	28,121–28,639	28,107–28,625	28,122-28,640	28,124–28,642
	20 kDa protein	28,669–29,208	28,655–29,194	28,670-29,209	28,672-29,211
E3	21.2 kDa protein	29,221–29,833	29,207–29,819	29,222–29,834	29,224–29,836
	8.8 kDa protein	29,863–30,089	29,849–30,075	29,864-30,090	29,866–30,092
	10.3 kDa protein	30,129–30,404	30,115–30,390	30,130–30,405	30,132–30,407
	16.6 kDa protein	30,376–30,813	30,362-30,799	30,377–30,814	30,379–30,816
	15.3 kDa protein	30,806–31,213	30,792–31,199	30,807–31,214	30,809–31,216
L5	fiber protein	31,411–32,382	31,397–32,368	31,412–32,383	31,414–32,385
	16 kDa protein	32,414–32,665; 33,388–33,561	32,400–32,651; 33,374–33,547	32,415–32,666; 33,389–33,562	32,417–32,668; 33,391–33,564
E4	34.7 kDa protein	32,662–3,3561	32,648–33,547	32,663–33,562	32,665–33,564
	14.3 kDa protein	33,464–33,832	33,450–33,818	33,465–33,833	33,467–33,835
L5	agnoprotein	33,687–34,196	33,673–34,182	33,688–34,197	33,690–34,199
	13.6 kDa protein	33,841–34,194	33,827–34,180	33,842–34,195	33,844–34,197
E4	14.4 kDa protein	34,191–34,580	34,177–34,566	34,192–34,581	34,194–34,583
	14.2 kDa protein	34,622–34,999	34,608–34,985	34,623–35,000	34,625–35,002

SUPPLEMENTARY TABLE S2-3. Genomic annotations of the strains Ningxia2024-674, Ningxia2024-725, Ningxia2024-747, and Ningxia2024-754.

Gene	Encoded product	Ningxia2024-674	Ningxia2024-725	Ningxia2024-747	Ningxia2024-754
	28.4 kDa protein	574–1,155;	575–1,156;	575–1,156;	575–1,156;
	26.4 KDa protein	1,249-1,452	1,250-1,453	1,250-1,453	1,250-1,453
E1A	24.6 kDa protein	574-1,062;	575-1,063;	575-1,063;	575-1,063;
LIA	24.0 KDa protein	1,249-1,452	1,250-1,453	1,250-1,453	1,250-1,453
	6.8 kDa protein	574–645;	575–646;	575–646;	575–646;
	0.0 KDa protein	1,247-1,348	1,248-1,349	1,248-1,349	1,248-1,349
E1B	small T antigen	1,600–2,136	1,601–2,137	1,601–2,137	1,601–2,137
LID	large T antigen (55K)	1,905–3,383	1,906–3,384	1,906–3,384	1,906–3,384
IX	hexon-associated protein IX	3,477-3,893	3,478-3,894	3,478-3,894	3,478-3,894
IVa2	maturation protoin IV/a2	3,946-5,279;	3947-5,280;	3,947-5,280;	3,947-5,280;
IVaz	maturation protein IVa2	5,558-5,570	5,559-5,571	5,559-5,571	5,559-5,571

Gene	Encoded product	Ningxia2024-674	Ningxia2024-725	Ningxia2024-747	Ningxia2024-75
	DNA polymerase	5,049–8,621; 13,839–13,847	5,050–8,622; 13,840–13,848	5,050–8,622; 13,841–13,849	5,050–8,622; 13,840–13,848
	hypothetical 11.5 kDa protein	6,142–,6462	6,143–6,463	6,143-6,463	6,143–6,463
	hypothetical 19 kDa protein	6,866–7,387	6,867–7,388	6,867–7,388	6,867-7,388
	hypothetical 10.4 kDa protein	7,131–7,418	7,132–7,419	7,132–7,419	7,132–7,419
E2B	DNA-binding protein	7,827–8,228; 9,478–9,495	7,828–8,229; 9,479–9,496	7,828–8,229; 9,479–9,496	7,828–8,229; 9,479–9,496
	hypothetical 12.6 kDa protein	8,227-8,571	8,228-8,572	8,228-8,572	8,228-8,572
	terminal protein precursor	8,420–10,387; 13,839–13,847	8,421–10,388; 13,840–13,848	8,421–10,388; 13,841–13,849	8,421–10,388; 13,840–13,848
	hypothetical 14.5 kDa protein	8,546-8,947	8,547-8,948	8,547-8,948	8,547-8,948
	hypothetical 11.5 kDa protein	9,541–9,855	9,542-9,856	9,542-9,856	9,542-9,856
	hypothetical 9.7 kDa protein	9,755–10,030	9,756-10,031	9,756-10,031	9,756-10,031
	52 kDa protein	10,856–12,025	10,857–12,026	10,858-12,027	10,857–12,026
L1	protein IIIa precursor	12,053–13,816	12,054–13,817	12,055–13,818	12,054–13,817
	penton protein	13,889–15,535	13,890–15,536	13,891–15,537	13,890–15,536
	protein VII precursor	15,549–16,127	15,548–16,126	15,551–16,129	15,548–16,126
L2	protein V precursor	16,167–17,228	16,166–17,227	16,169–17,230	16,166–17,227
	protein X	17,257–17,487	17,256–17,486	17,259–17,489	17,256–17,486
	protein VI precursor	17,560–18,309	17,559–18,308	17,562–18,311	17,559–18,308
L3	hexon protein	18,426–21,275	18,422–21,271	18,425–21,274	18,422–21,27
	23 kDa proteinase	21,312–21,941	21,308–21,937	21,311–21,940	21,308–21,93
Ξ2A	DNA-binding protein	22,030–23,583	22,026–23,579	22,029–23,582	22,026–23,579
, \	100 kDa hexon-assembly associated protein	23,614–26,097	23,610–26,093	23,613–26,096	23,610–26,09
	33 kDa protein	25,799–26,672	25,795–26,668	25,798–26,671	25,795–26,668
L4	22 kDa protein	25,799–26,398	25,795–26,394	25,798–26,397	25,795–26,394
	protein VIII	26,743–27,426	26,739–27,422	26,742–27,425	26,739–27,422
	12.1 kDa protein	27,426–27,746	27,422–27,742	27,425–27,745	27,422–27,742
	·		,	27,699–28,139	
	16 kDa protein	27,700–28,140	27,696–28,136		27,696–28,130
	19.2 kDa protein	28,125–28,643	28,121–28,639	28,124–28,642	28,121–28,63
- 0	20 kDa protein	28,673–29,212	28,669–29,208	28,672–29,211	28,669–29,20
E3	21.2 kDa protein	29,225–29,837	29,221–29,833	29,224–29,836	29,221–29,83
	8.8 kDa protein	29,867–30,093	29,863–30,089	29,866–30,092	29,863–30,089
	10.3 kDa protein	30,133–30,408	30,129–30,404	30,132–30,407	30,129–30,40
	16.6 kDa protein	30,380–30,817	30,376–30,813	30,379–30,816	30,376–30,81
	15.3 kDa protein	30,810–31,217	30,806–31,213	30,809–31,216	30,806–31,21
L5	fiber protein	31,415–32,386	31,411–32,382	31,414–32,385	31,411–32,38
	16 kDa protein	32,418–32,669; 33,392–33,565	32,414–32,665; 33,388–33,561	32,417–32,668; 33,391–33,564	32,414–32,665 33,388–33,56
E4	34.7 kDa protein	32,666–33,565	32,662–33,561	32,665–33,564	32,662–33,56
	14.3 kDa protein	33,468–33,836	33,464–33,832	33,467–33,835	33,464–33,83
L5	agnoprotein	33,691–34,200	33,687–34,196	33,690–34,199	33,687–34,19
	13.6 kDa protein	33,845–34,198	33,841–34,194	33,844–34,197	33,841–34,19
E4	14.4 kDa protein	34,195–34,584	34,191–34,580	34,194–34,583	34,191–34,580
	14.2 kDa protein	34,626–35,003	34,622–34,999	34,625–35,002	34,622–34,999

China CDC Weekly

SUPPLEMENTARY TABLE S2-4. Genomic annotation of strains Ningxia2024-868, Ningxia2024-907, Ningxia2024-944, and Beijing2024-330.

Gene	Encoded product	Ningxia2024-868	Ningxia2024-907	Ningxia2024-944	Beijing2024-33
	28.4 kDa protein	575–1,156;	575–1,156;	576–1,148;	567–1,148;
		1,250–1,453 575–1,063;	1,250–1,453 575–1,063;	1,242–1,445 576–1,064;	1,242–1,445 567–1,055;
E1A	24.6 kDa protein	1,250–1,453	1,250–1,453	1,242–1,445	1,242–1,445
	6.9 kDa protoin	575–646;	575–646;	567–638;	567–638;
	6.8 kDa protein	1,248–1,349	1,248–1,349	1,240–1,341	1,240–1,341
E1B	small T antigen	1,601–2,137	1,601–2,137	1,593–2,129	1,593–2,129
2.5	large T antigen (55K)	1,906–3,384	1,906–3,384	1,898–3,376	1,898–3,376
IX	hexon-associated protein IX	3,478–3,894	3,478–3,894	3,470–3,886	3,470–3,886
IVa2	maturation protein IVa2	3,947–5,280; 5,559–5,571	3,947–5,280; 5,559–5,571	3,939–5,272; 5,551–5,563	3,939–5,272; 5,551–5,563
	DNA polymerase	5,050–8,622; 13,840–13,848	5,050–8,622; 13,841–13,849	5,042–8,614; 13,831–13,839	5,042–8,614; 13,832–13,840
	hypothetical 11.5 kDa protein	6,143–6,463	6,143–6,463	6,135–6,455	6,135–6,455
	hypothetical 19 kDa protein	6,867–7,388	6,867–7,388	6,859–7,380	6,859–7,380
	hypothetical 10.4 kDa protein	7,132–7,419	7,132–7,419	7,124–7,411	7,124–7,411
E2B	DNA-binding protein	7,828–8,229; 9,479–9,496	7,828–8,229; 9,479–9,496	7,820–8,221; 9,471–9,488	7,820–8,221; 9,471–9,488
LZD	hypothetical 12.6 kDa protein	8,228-8,572	8,228-8,572	8,220-8,564	8,220-8,564
	terminal protein precursor	8,421–10,388; 13,840–13,848	8,421–10,388; 13,841–13,849	8,413–10,380; 13,831–13,839	8,413–10,380; 13,832–13,840
	hypothetical 14.5 kDa protein	8,547-8,948	8,547-8,948	8,539-8,940	8,539–8,940
	hypothetical 11.5 kDa protein	9,542–9,856	9,542-9,856	9,534–9,848	9,534–9,848
	hypothetical 9.7 kDa protein	9,756–10,031	9,756–10,031	9,748-10,023	9,748–10,023
1.4	52 kDa protein	10,857–12,026	10,858-12,027	10,848–12,017	10,849–12,018
L1	protein IIIa precursor	12,054–13,817	12,055–13,818	12,045–13,808	12,046–13,809
	penton protein	13,890–15,536	13,891–15,537	13,881–15,527	13,882–15,53
L2	protein VII precursor	15,548–16,126	15,549–16,127	15,539–16,117	15,540–16,11
LZ	protein V precursor	16,166–17,227	16,167–17,228	16,157–17,218	16,158–17,21
	protein X	17,256–17,486	17,257–17,487	17,247–17,477	17,248–17,47
	protein VI precursor	17,559–18,308	17,560–18,309	17,550–18,299	17,551–18,30
L3	hexon protein	18,422–21,271	18,423–21,272	18,413–21,262	18,414–21,26
	23 kDa proteinase	21,308–21,937	21,309–21,938	21,299–21,928	21,300–21,92
E2A	DNA-binding protein	22,026–23,579	22,027–23,580	22,017–23,570	22,018–23,57
	100 kDa hexon-assembly associated protein	23,610–26,093	23,611–26,094	23,601–26,084	23,602–26,08
1.4	33 kDa protein	25,795–26,668	25,796–26,669	25,786–26,659	25,787–26,66
L4	22 kDa protein	25,795–26,394	25,796–26,395	25,786–26,385	25,787–26,38
	protein VIII	26,739–27,422	26,740-27,423	26,730–27,413	26,731–27,41
	12.1 kDa protein	27,422–27,742	27,423–27,743	27,413–27,733	27,414–27,73
	16 kDa protein	27,696–28,136	27,697–28,137	27,687–28,127	27,688–28,128
	19.2 kDa protein	28,121–28,639	28,122-28,640	28,112–28,630	28,113–28,63
	20 kDa protein	28,669–29,208	28,670-29,209	28,660–29,199	28,661–29,200
E3	21.2 kDa protein	29,221–29,833	29,222-29,834	29,212–29,824	29,213–29,82
	8.8 kDa protein	29,863–30,089	29,864-30,090	29,854-30,080	29,855–30,08
	10.3 kDa protein	30,129-30,404	30,130-30,405	30,120-30,395	30,121–30,396
	16.6 kDa protein	30,376–30,813	30,377–30,814	30,367–30,804	30,368–30,80
	15.3 kDa protein	30,806–31,213	30,807-31,214	30,797–31,204	30,798–31,205

Gene	Encoded product	Ningxia2024-868	Ningxia2024-907	Ningxia2024-944	Beijing2024-330
L5	fiber protein	31,411–32,382	31,412–32,383	31,402–32,373	31,403–32,374
	16 kDa protein	32,414–32,665; 33,388–33,561	32,415–32,666; 33,389–33,562	32,405–32,656; 33,379–33,552	32,406–32,657; 33,380–33,553
E4	34.7 kDa protein	32,662-33,561	32,663–33,562	32,653–33,552	32,654–33,553
	14.3 kDa protein	33,464–33,832	33,465–33,833	33,455–33,823	33,456–33,824
L5	agnoprotein	33,687–34,196	33,688–34,197	33,678–34,187	33,679–34,188
	13.6 kDa protein	33,841–34,194	33,842–34,195	33,832–34,185	33,833–34,186
E4	14.4 kDa protein	3,4191–34,580	34,192–34,581	34,182–34,571	34,183–34,572
	14.2 kDa protein	34,622-34,999	34,623–35,000	34,613–34,990	34,614–34,991

SUPPLEMENTARY TABLE S2-5. Genomic annotation of strains Beijing2024-364, Beijing2024-378, Shenzhen2024-077, and Shenzhen2024-201.

Gene	Encoded product	Beijing2024-364	Beijing2024-378	Shenzhen2024-077	Shenzhen2024-201
	28.4 kDa protein	575–1,156;	575–1,156;	575–1,156;	566–1,147;
	20.1 KBa protom	1,250–1,453	1,250–1,453	1,250–1,453	1,241–1,444
E1A	24.6 kDa protein	575–1,063; 1,250–1,453	575–1,063; 1,250–1,453	575–1,063; 1,250–1,453	566–1,054; 1,241–1,444
		575–646;	575–646;	575–646;	566–637;
	6.8 kDa protein	1,248–1,349	1,248–1,349	1,248–1,349	1,239–1,340
E4D	small T antigen	1,601–2,137	1,601–2,137	1,601–2,137	1,592–2,128
E1B	large T antigen (55K)	1,906–3,384	1,906–3,384	1,906–3,384	1,897–3,375
IX	hexon-associated protein IX	3,478–3,894	3,478–3,894	3,478-3,894	3,469–3,885
IVa2	maturation protein IVa2	3,947-5,280;	3,947-5,280;	3,947-5,280;	3,938–5,271;
1742	mataration protein rvaz	5,559–5,571	5,559–5,571	5,559–5,571	5,550-5,562
	DNA polymerase	5,050–8,622;	5,050–8,622;	5,050–8,622;	5,041–8,613;
		1,3841–1,3849	13,841–13,849	13,841–13,849	13,833–13,841
	hypothetical 11.5 kDa protein	6,143–6,463	6,143–6,463	6,143–6,463	6,134–6,454
	hypothetical 19 kDa protein	6,867–7,388	6,867–7,388	6,867–7,388	6,858–7,379
	hypothetical 10.4 kDa protein	7,132–7,419	7,132–7,419	7,132–7,419	7,123–7,410
	DNA-binding protein	7,828–8,229;	7,828–8,229;	7,828–8,229;	7,819–8,220;
E2B		9,479–9,496	9,479–9,496	9,479–9,496	9,470–9,487
	hypothetical 12.6 kDa protein	8,228–8,572	8,228–8,572	8,228-8,572	8,219–8,563
	terminal protein precursor	8,421–10,388;	8421–10,388;	8,421–10,388;	8,412–10,379;
	terriiriai proteiri precursor	13,841–13,849	13,841–13,849	13,841–13,849	13,833–13,841
	hypothetical 14.5 kDa protein	8,547–8,948	8,547–8,948	8,547–8,948	8,538–8,939
	hypothetical 11.5 kDa protein	9,542–9,856	9,542–9,856	9,542–9,856	9,533–9,847
	hypothetical 9.7 kDa protein	9,756–10,031	9,756–10,031	9,756–10,031	9,747–10,022
L1	52 kDa protein	10,858–12,027	10,858–12,027	10,858–12,027	10,850–12,019
LI	protein Illa precursor	12,055–13,818	12,055–13,818	12,055–13,818	12,047-13,810
	penton protein	13,891–15,540	13,891–15,540	13,891–15,537	13,883–15,529
	protein VII precursor	15,549–16,127	15,549–16,127	15,549–16,127	15,540–16,118
L2	protein V precursor	16,167–17,228	16,167–17,228	16,167–17,228	16,158–17,219
	protein X	17,257–17,487	17,257–17,487	17,257–17,487	17,248–17,478
	protein VI precursor	17,560–18,309	17,560–18,309	17,560–18,309	17,551–18,300
L3	hexon protein	18,423–21,272	18,423–21,272	18,423–21,272	18,417–21,266
	23 kDa proteinase	21,309–21,938	21,309–21,938	21,309–21,938	21,303–21,932
E2A	DNA-binding protein	22,027-23,580	22,027-23,580	22,027-23,580	22,021–23,574

Gene	Encoded product	Beijing2024-364	Beijing2024-378	Shenzhen2024-077	Shenzhen2024-201
	100 kDa hexon-assembly associated protein	23,611–26,094	23,611–26,094	23,611–26,094	23,605–26,088
L4	33 kDa protein	25,796–26,669	25,796–26,669	25,796–26,669	25,790–26,663
L4	22 kDa protein	25,796–26,395	25,796–26,395	25,796–26,395	25,790–26,389
	protein VIII	26,740-27,423	26,740-27,423	26,740-27,423	26,734–27,417
	12.1 kDa protein	27,423–27,743	27,423–27,743	27,423–27,743	27,417–27,737
	16 kDa protein	27,697–28,137	27,697–28,137	27,697–28,137	27,691–28,131
	19.2 kDa protein	28,122-28,640	28,122-28,640	28,122-28,640	28,116–28,634
	20 kDa protein	28,670-29,209	28,670–29,209	28,670-29,209	28,664–29,203
E3	21.2 kDa protein	29,222-29,834	29,222-29,834	29,222-29,834	29,216–29,828
	8.8 kDa protein	29,864-30,090	29,864-30,090	29,864-30,090	29,858-30,084
	10.3 kDa protein	30,130-30,405	30,131–30,406	30,130-30,405	30,124-30,399
	16.6 kDa protein	30,377–30,814	30,378–30,815	30,377-30,814	30,371–30,808
	15.3 kDa protein	30,807–31,214	30,808–31,215	30,807-31,214	30,801–31,208
L5	fiber protein	31,412–32,383	31,413–32,384	31,412–32,383	31,406–32,377
	16 kDa protein	32,415–32,666; 33,389–33,562	32,416–32,667; 33,390–33,563	32,415–32,666; 33,389–33,562	32,409–32,660; 33,383–33,556
E4	34.7 kDa protein	32,663–33,562	32,664–33,563	32,663-33,562	32,657–33,556
	14.3 kDa protein	33,465–33,833	33,466–33,834	33,465–33,833	33,459–33,827
L5	agnoprotein	33,688–34,197	33,689–34,198	33,688–34,197	33,682–34,191
	13.6 kDa protein	33,842–34,195	33,843–34,196	33,842–34,195	33,836–34,189
E4	14.4 kDa protein	34,192–34,581	34,193–34,582	34,192–34,581	34,186–34,575
	14.2 kDa protein	34,623-35,000	34,624-35,001	34,623-35,000	34,617-34,994

SUPPLEMENTARY TABLE S2-6. Genomic annotations of strains Chongqing2024-069, Shenyang2024-163, and Gansu2024-215.

Gene	Encoded product	Chongqing2024-069	Shenyang2024-163	Gansu2024-215
	28.4 kDa protein	575–,1156;	575–1,156;	575–1,156;
	20.4 KDa proteiri	1,250–1,453	1,250–1,453	1250-1,453
E1A	24.6 kDa protein	575–1,063;	575–1,063;	575–1,063;
, \	2 1.0 KBa protom	1,250–1,453	1,250–1,453	1,250–1,453
	6.8 kDa protein	575–646;	575–646;	575–646;
	· .	1,248–1,349	1,248–1,349	1,248–1,349
E1B	small T antigen	1,601–2,137	1,601–2,137	1,601–2,137
LID	large T antigen (55K)	1,906–3,384	1,906–3,384	1,906–3,384
IX	hexon-associated protein IX	3,478-3,894	3,478-3,894	3,478-3,894
IVa2	maturation protein IVa2	3,947–5,280;	3,947–5,280;	3,947-5,280;
IVaZ	maturation protein rvaz	5,559–5,571	5,559–5,571	5,559-5,571
	DNA polymerase	5,050-8,622;	5,050-8,622;	5,050-8,622;
	DIVA polymerase	13,841–13,849	13,841–13,849	13,841–13,849
	hypothetical 11.5 kDa protein	6,143–6,463	6,143–6,463	6,143–6,463
	hypothetical 19 kDa protein	6,867–7,388	6,867–7,388	6,867–7,388
	hypothetical 10.4 kDa protein	7,132–7,419	7,132–7,419	7,132–7,419
	DNA hinding protoin	7,828-8,229;	7,828-8,229;	7,828-8,229;
E2B	DNA-binding protein	9,479–9,496	9,479–9,496	9,479-9,496
	hypothetical 12.6 kDa protein	8,228-8,572	8,228-8,572	8,228-8,572
		8,421-10,388;	8,421–10,388;	8,421-10,388;
	terminal protein precursor	13,841-13,849	13,841-13,849	13,841-13,849
	hypothetical 14.5 kDa protein	8,547-8,948	8,547-8,948	8,547-8,948
	hypothetical 11.5 kDa protein	9,542–9,856	9,542–9,856	9,542-9,856
	hypothetical 9.7 kDa protein	9,756–10,031	9,756–10,031	9,756–10,031

China CDC Weekly

Continued

Gene	Encoded product	Chongqing2024-069	Shenyang2024-163	Gansu2024-215
L1	52 kDa protein	10,858–12,027	10,858–12,027	10,858–12,027
LI	protein IIIa precursor	12,055–13,818	12,055–13,818	12,055–13,818
	penton protein	13,891–15,540	13,891–15,537	13,891–15,537
L2	protein VII precursor	15,549–16,127	15,549–16,127	15,549–16,127
LZ	protein V precursor	16,167–17,228	16,167–17,228	16,167–17,228
	protein X	17,257–17,487	17,257–17,487	17,257–17,487
	protein VI precursor	17,560–18,309	17,560–18,309	17,560–18,309
L3	hexon protein	18,423–21,272	18,423–21,272	18,423–21,272
	23 kDa proteinase	21,309–21,938	21,309–21,938	21,309–21,938
E2A	DNA-binding protein	22,027–23,580	22,027–23,580	22,027–23,580
	100 kDa hexon-assembly associated protein	23,611–26,094	23,611–26,094	23,611–26,094
1.4	33 kDa protein	25,796–26,669	25,796–26,669	25,796–26,669
L4	22 kDa protein	25,796–26,395	25,796–26,395	25,796–26,395
	protein VIII	26,740–27,423	26,740–27,423	26,740–27,423
	12.1 kDa protein	27,423–27,743	27,423–27,743	27,423–27,743
	16 kDa protein	27,697–28,137	27,697–28,137	27,697–28,137
	19.2 kDa protein	28,122-28,640	28,122-28,640	28,122–28,640
	20 kDa protein	28,670–29,209	28,670-29,209	28,670-29,209
E3	21.2 kDa protein	29,222–29,834	29,222–29,834	29,222–29,834
	8.8 kDa protein	29,864-30,090	29,864-30,090	29,864-30,090
	10.3 kDa protein	30,130–30,405	30,130-30,405	30,130–30,405
	16.6 kDa protein	30,377–30,814	30,377–30,814	30,377–30,814
	15.3 kDa protein	30,807–31,214	30,807-31,214	30,807–31,214
L5	fiber protein	31,412–32,383	31,412–32,383	31,412–32,383
	16 kDa protein	32,415–32,666;	32,415–32,666;	32,415–32,666;
E4	34.7 kDa protein	33,389–33,562 32,663–33,562	33,389–33,562 32,663–33,562	33,389–33,562 32,663–33,562
	14.3 kDa protein	33,465–33,833	33,465–33,833	33,465–33,833
L5	agnoprotein	33,688–34,197	33,688–34,197	33,688–34,197
	13.6 kDa protein	33,842–34,195	33,842–34,195	33,842–34,195
E4	14.4 kDa protein	34,192–34,581	34,192–34,581	34,192–34,581
	14.2 kDa protein	34,623–35,000	34,623–35,000	34,623–35,000

Preplanned Studies

Detection of Dengue Virus RNA in Breast Milk Following Peripartum Infection — Guangzhou City, Guangdong Province, China, 2024

Fang Peng^{1,&}; Yuanjing Xu^{1,2,&}; Minghao Li¹; Zhixi Tan¹; Yuyan Lin¹; Jianting Chen¹; Yongliang Ou¹; Shuxian Pan^{1,#}

Summary

What is already known about this topic?

Dengue fever is primarily transmitted by Aedes mosquitoes. While most cases are asymptomatic or mild, some may progress to severe complications. Laboratory diagnosis relies on detection of nucleic acid, antigen, or antibodies in blood specimens.

What is added by this report?

A patient who developed dengue fever 1 day before delivery had dengue virus RNA, NS1 antigen, and IgM detected in breast milk within 10 days of symptom onset. Nucleic acid and NS1 turned negative by day 15, while IgM antibodies remained positive and turned negative by day 22, suggesting potential transmission risk via early breastfeeding.

What are the implications for public health practice?

Breastfeeding should be avoided until 22 days postonset, after confirming clearance of viral RNA and IgM from breast milk and excluding infection in the infant. Household members of pregnant women exhibiting suspected dengue symptoms should seek immediate medical attention for dengue NS1 antigen testing during dengue season.

ABSTRACT

Introduction: Through analysis of a dengue-infected patient presenting symptom 1 day before delivery, this study evaluated the risk of vertical dengue virus transmission through breast feeding. By assessing breastfeeding-associated risks and benefits, this study may inform breastfeeding guidelines for dengue-infected mothers.

Methods: Breast milk samples were collected 10, 15, and 22 days after onset. Field epidemiological investigations and comprehensive laboratory analyses of blood and breast milk samples were conducted, followed by whole-genome viral sequencing using

nanopore technology.

Results: Within 10 days of disease onset, dengue virus RNA, NS1 antigen, and IgM in breast milk were all positive (nucleic acid Ct value: 35.58), whereas IgG was negative. Dengue virus RNA, NS1 antigen, and IgG in breast milk were negative on the 15th day of onset, while IgM was negative until the 22nd day of onset. Phylogenetic tree analysis of the whole genome showed that this strain was most closely related to the Guangdong isolate (PP563845.1), with 99.90% homology.

Conclusion: Early breastfeeding by patients with dengue fever during late gestation may pose a risk of viral transmission. Breastfeeding should be cautiously initiated 22 days post-onset only after confirming that both breast milk nucleic acid and IgM have seroconverted to a negative status.

Dengue fever is an acute infectious disease caused by the dengue virus. The virus is mainly transmitted by Aedes mosquitoes, making dengue fever a self-limiting disease. While most infections are asymptomatic or cause mild febrile illness, a subset of patients may progress to severe complications, including dengue hemorrhagic fever and dengue shock syndrome (1). The subtropical climate of Guangdong Province fosters optimal conditions for Aedes mosquito proliferation, establishing an ecological foundation for sustained dengue fever transmission. Since Guangzhou's first case of dengue fever reported in 1978 (2), it has become one of the main epidemic areas in China. Dengue virus includes four serotypes: DENV1 to DENV4 (3).

Although previous studies have elucidated the transmission pathways of dengue fever, research on breast milk as a potential diagnostic specimen remains limited. To address this knowledge gap, this study investigated the risk of vertical dengue virus transmission through the colostrum breast milk of a

pregnant woman who developed dengue fever during late gestation. The findings of the study may help refine breastfeeding recommendations for this demographic.

A 35-year-old unemployed Chinese woman, residing with her mother and husband in a city near Guangzhou, presented with a fever (37.8 °C) on November 21, 2024. Her mother and husband had been diagnosed with dengue fever in early November 2024 and received treatment at a local hospital. The patient was hospitalized on November of 22 with a body temperature of 38.9 °C, pulse rate of 136 bpm, respiratory rate of 22 breaths/min, blood pressure of 94/64 mmHg, white blood cell count of 6.66×10⁹/L, and platelet count of 205×10⁹/L, with no apparent rash. An epidemiological investigation revealed that her activities were limited to her residential area 14 days before the symptom onset. Her household had mosquito nets, ornamental plant cultivation and a rooftop vegetable garden, with self-reported frequent mosquito infestations. On the day of hospitalization, the patient underwent an epidural anesthesia-assisted cesarean section to deliver a male infant. Postoperative body temperature fluctuated between 35.8 °C and 39.4 °C, and a chest X-ray ruled out pneumonia.

Breast milk samples were collected 10, 15, and 22 days after onset. Dengue virus testing of maternal blood on November 22 showed positive nucleic acid (nucleic acid Ct value: 24.9) and NS1 antigen, but negative IgM and IgG in the patient. The newborn tested negative for NS1, IgM, and IgG on November 23, and subsequent testing on November 28 revealed negative nucleic acids and NS1, with a clinical presentation of petechiae but no fever. Within 10 days of onset (November 30), dengue virus RNA, NS1 antigen, and IgM in breast milk were all positive (nucleic acid Ct value: 35.58), whereas IgG was negative. Dengue virus RNA, NS1 antigen, and IgG in breast milk were negative on the 15th day of onset (December 5), whereas IgM was negative until the 22nd day of onset (December 12). The patient was discharged on November 28, with follow-up on December 5 showing a white blood cell count of 7.99×10⁹/L and platelets of 471×10⁹/L. Breastfeeding initiation was not suggested for this patient until all breast milk biomarkers yielded laboratory-confirmed negative results (Table 1).

The patient was diagnosed with DENV serotype-1 through dengue viral RNA detection using a reverse transcription-polymerase chain reaction (RT-PCR) assay. Third-generation nanopore sequencing

successfully yielded a 10.7 kb viral genomic sequence. BLAST analysis revealed that the nucleotide homology of this strain with the reference (NC001477.1) sequence was 92.46% and exhibited high similarity (99.90%) with the 2023 Guangdong isolate (PP563845.1), with only one amino acid differential site (L617S) in the E protein region of the isolates. Phylogenetic analysis (Figure 1) showed

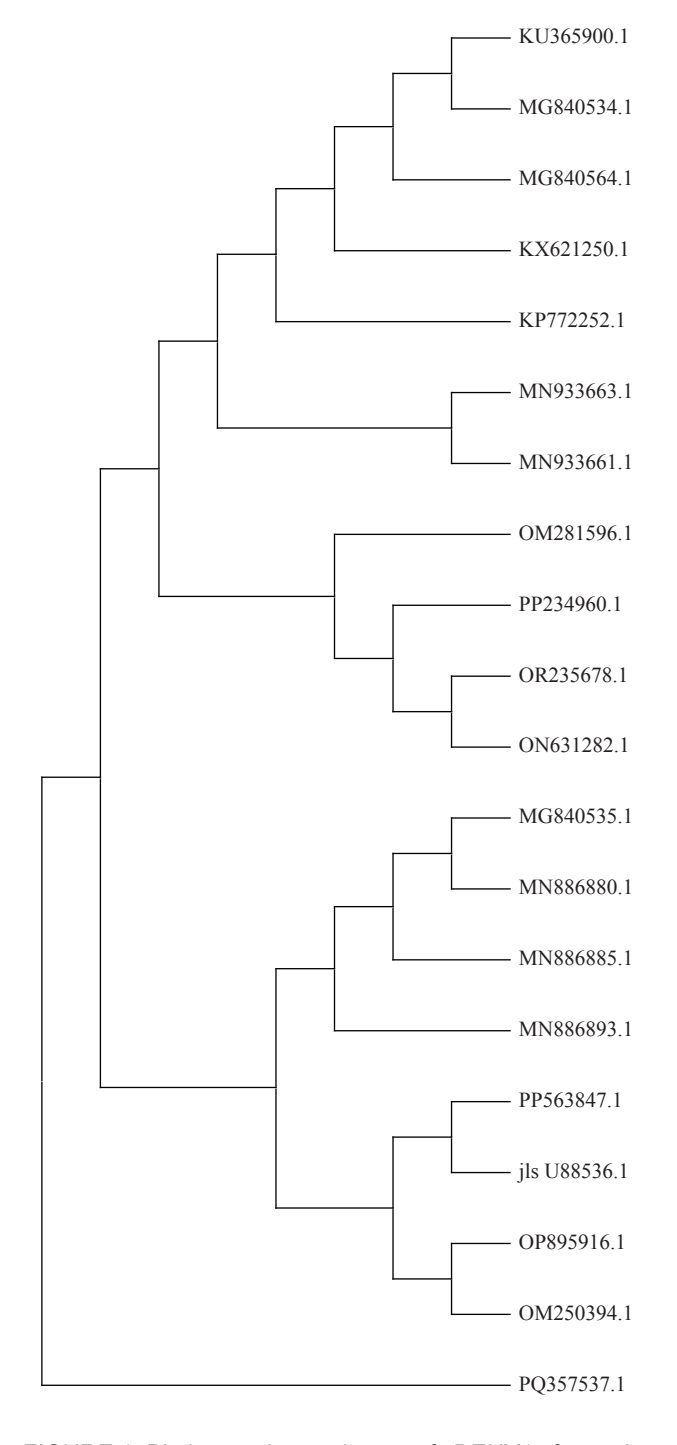


FIGURE 1. Phylogenetic analyses of DENV1 from the patient.

TABLE 1. Results of dengue virus serological and breast milk tests in mother patient.

	Project									
Sampling date	Sera				Breast milk					
	Nucleic acid	NS1	IgM	IgG	Nucleic acid	NS1	IgM	IgG		
November 22 (2 days post-onset)	Positive (Ct: 24.9)	Positive	Negative	Negative	1	/	1	1		
November 30 (10 days post-onset)	1	1	1	1	Positive (Ct:35.58)	Positive	Positive	Negative		
December 5 (15 days post-onset)	1	1	1	1	Negative	Negative	Positive	Negative		
December 12 (22 days post-onset)	1	1	1	1	Negative	Negative	Negative	Negative		

Note: /, No detection.

98.86%–99.90% homology with isolates from Southeast Asian countries, suggesting that this epidemic may be related to imported cases (4–6).

DISCUSSION

To the best of our knowledge, this study documents the first confirmed detection of persistent dengue viral RNA in postpartum breast milk in China, which was identified within 10 days of the onset of maternal symptoms. Our integrated epidemiological and laboratory evidence demonstrates that perinatal dengue infections may pose dual health risks through both vertical transmission and breastfeeding exposure pathways.

Arragain et al. found that the nucleic acid of the dengue virus was present in breast milk; the viral genome was detected in breast milk 1-14 days after disease onset (7). This finding is similar to that of our study, suggesting that breast milk may be a potential route of neonatal infection. Barthel et al. reported a case of vertical transmission of dengue fever; the virus was detected in continuous blood samples from the mother and infant as well as in breast milk, raising concerns about the risk of transmission of dengue fever to newborns during breastfeeding (8). Wang et al. demonstrated that while newborns infected with dengue fever in late gestation may not show severe manifestations of dengue hemorrhagic fever, there is still a risk of vertical transmission of the dengue virus (9). It has been reported that in cases of vertical transmission, maternal infection can lead to viremia, resulting in IgM-positive responses in both mothers and newborns (10). Studies indicate that IgM antibodies against human immunodeficiency viruses, Zika virus, and cytomegalovirus can be transmitted through breast milk, and the persistence of IgM antibodies may pose potential risks to neonates (11).

Biomarker testing revealed that the patient's breast milk was positive for IgM but negative for IgG on the 10th day post-symptom onset, with persistent IgM positivity observed until day 15, indicating an incomplete or transient immune response following acute infection. The World Health Organization and United Nations Children's Fund recommend that children initiate breastfeeding within the first hour of birth and be exclusively breastfed for the first 6 months of life (12). Our findings highlight the potential risk of vertical transmission via breastfeeding during the period of detectable dengue viral RNA in breast milk. Based on the case-specific results of this study, breastfeeding should be cautiously initiated 22 days post-onset only after confirming that both breast milk nucleic acids and IgM have seroconverted to negative status, with concurrent verification of infant afebrile status, absence of cutaneous eruptions, and laboratory exclusion of dengue infection. Notably, Lee et al. showed that maternally transferred dengue-specific IgG antibodies via breastfeeding not only extended the disease enhancement window in murine models, but also provided protection against homologous viral challenge (13). The identification of breast milk components that enable neutralizing antibody transfer while facilitating viral transmission provides crucial evidence supporting the need to update breastfeeding recommendations, particularly for convalescent mothers in dengue hyperendemic regions. An early study reported the anti-dengue activity of the lipid components of human milk and colostrum. This suggests that breastfeeding protects infants from the dengue virus in dengue-endemic areas (14).

The findings in this report are subject to at least four limitations. First, direct evidence of vertical transmission through breastfeeding could not be established, because the newborn was not breastfed during the study period and tested negative for the

virus. Second, the absence of placental tissue and cord blood samples precluded further investigation of potential transmission mechanisms. Third, the newborn had petechiae but no fever, with negative nucleic acid and NS1; therefore, we did not proceed with further dengue testing for the infant. This presentation may be because severe dengue infections lead to endothelial damage and increased vascular permeability (15). Finally, because this evidence stems from an isolated case report, its generalizability to a broader population remains unclear. Consequently, our findings should be interpreted with caution, and further studies with a more complete sample collection are needed to fully evaluate the risk-benefit ratio of breastfeeding in dengue-infected mothers.

In conclusion, this study revealed that there may be a risk of viral transmission during early breastfeeding for patients infected with dengue fever in late gestation. Based on this individual case, cautious breastfeeding after ruling out clinical symptoms of dengue infection in both mothers and infants may help prevent viral transmission and poor health outcomes. During seasonal transmission periods in dengue-endemic regions, household members of pregnant women exhibiting suspected dengue symptoms should seek immediate medical attention for dengue NS1 antigen testing. Additionally, future breastfeeding guidelines should incorporate biomarker testing to safeguard maternal-infant health.

Conflicts of interest: No conflicts of interest.

Acknowledgements: The patient for participating in the study.

Ethical statement: Approval from the institutional review board of Guangzhou Center for Disease Control and Prevention (No.: [PJ2025004]) on May 28th, 2025.

Funding: Supported by the Guangzhou Health Science and Technology Project (20241A010094).

doi: 10.46234/ccdcw2025.229

Copyright © 2025 by Chinese Center for Disease Control and Prevention. All content is distributed under a Creative Commons Attribution Non Commercial License 4.0 (CC BY-NC).

Submitted: June 11, 2025 Accepted: October 16, 2025 Issued: October 24, 2025

REFERENCES

- Deng J, Zhang H, Wang YP, Liu Q, Du M, Yan WX, et al. Global, regional, and national burden of dengue infection in children and adolescents: an analysis of the Global Burden of Disease Study 2021. eClinicalMedicine 2024;78:102943. https://doi.org/10.1016/j.eclinm. 2024.102943.
- Liu ZW, Yu YX, Jia LL, Dong GM, Wang ZW. Sequence determination and phylogenetic analysis of two dengue virus type 4 Strains isolated in the first outbreak of dengue fever after the foundation of the People's Republic of China. Chin J Zoonoses 2007;23(7):678 – 82,86. https://doi.org/10.3969/j.issn.1002-2694.2007.07.012.
- Li ZW, Huang XX, Li AQ, Du SS, He GX, Li JD. Epidemiological characteristics of dengue fever-China, 2005-2023. China CDC Wkly 2024;6(41):1045 – 8. https://doi.org/10.46234/ccdcw2024.217.
- Lun XC, Wang YG, Zhao CC, Wu HX, Zhu CY, Ma DL, et al. Epidemiological characteristics and temporal-spatial analysis of overseas imported dengue fever cases in outbreak provinces of China, 2005-2019. Infect Dis Poverty 2022;11(1):12. https://doi.org/10.1186/ s40249-022-00937-5.
- Sang SW, Chen B, Wu HX, Yang ZC, Di B, Wang LH, et al. Dengue is still an imported disease in China: a case study in Guangzhou. Infect Genet Evol 2015;32:178 – 90. https://doi.org/10.1016/j.meegid.2015. 03.005
- Yue YJ, Liu XB, Guo YH, Zhao N, Ren DS, Liu QY. Spatio-temporal distribution and environmental factors of dengue fever in China, 2020– 2022. J Environ Hyg 2023;5(13):341 – 5. https://doi.org/10.13421/j. cnki.hjwsxzz.2023.05.006.
- Arragain L, Dupont-Rouzeyrol M, O'Connor O, Sigur N, Grangeon JP, Huguon E, et al. Vertical transmission of dengue virus in the peripartum period and viral kinetics in newborns and breast milk: new data. J Pediatric Infect Dis Soc 2017;6(4):324 31. https://doi.org/10.1093/jpids/piw058.
- Barthel A, Gourinat AC, Cazorla C, Joubert C, Dupont-Rouzeyrol M, Descloux E. Breast milk as a possible route of vertical transmission of dengue virus. Clin Infect Dis 2013;57(3):415 – 7. https://doi.org/10. 1093/cid/cit227.
- Wang JP, Zhang Y, Nie C, Gao WW, Shuai C, Lin QQ, et al. Neonatal dengue fever: four cases report. J Clin Pediatr 2016;34(9):661

 3. https://doi.org/10.3969/j.issn.1000-3606.2016.09.005.
- Bhattarai CD, Yadav BK, Basnet R, Karki M, Chauhan S. Dengue fever in a neonate: a case report. JNMA J Nepal Med Assoc 2022;61(259): 287 – 9. https://doi.org/10.31729/jnma.8099.
- 11. Desgraupes S, Hubert M, Gessain A, Ceccaldi PE, Vidy A. Mother-to-child transmission of arboviruses during breastfeeding: from epidemiology to cellular mechanisms. Viruses 2021;13(7):1312. https://doi.org/10.3390/v13071312.
- WHO. 2025. Global health organization. https://www.who.int/health-topics/breastfeeding#tab=tab_2. [2025-7-11]
- 13. Lee PX, Ong LC, Libau EA, Alonso S. Relative contribution of dengue IgG antibodies acquired during gestation or breastfeeding in mediating dengue disease enhancement and protection in type I interferon receptor-deficient mice. PLoS Negl Trop Dis 2016;10(6):e0004805. https://doi.org/10.1371/journal.pntd.0004805.
- Chong KY, Lin KC. A preliminary report of the fetal effects of dengue infection in pregnancy. Gaoxiong J Med Sci 1989;5(1):31-4.
- Rathore SS, Oberoi S, Hilliard J, Raja R, Ahmed NK, Vishwakarma Y, et al. Maternal and foetal-neonatal outcomes of dengue virus infection during pregnancy. Trop Med Int Health 2022;27(7):619 – 29. https:// doi.org/10.1111/tmi.13783.

[#] Corresponding author: Shuxian Pan, lwcdcyz@gz.gov.cn.

¹ Guangzhou Liwan Center for Disease Control and Prevention, Guangzhou City, Guangdong Province, China; ² Bomi Center for Disease Control and Prevention, Nyingchi City, Xizang Autonomous Region, China.

[&]amp; Joint first authors.

Preplanned Studies

Prospective Study on Clinical Performance of Host DNA Methylation Assay for Triage in Women Who Are HPV-Positive — 4 Provinces, China, 2018–2021

Jing Zhang^{1,&}; Jinxueyue Chen^{2,&}; Hui Feng¹; Ying Hong³; Jing Zhao⁴; Xiaohua Pan⁵; Yan Chen⁵; Jian Zhao¹; Yan Zhang^{1,#}

Summary

What is already known about this topic?

Persistent infection with high-risk human papillomavirus (hrHPV) is recognized as the primary cause of cervical cancer and its precancerous lesions. However, most HPV infections are transient and naturally clear. Currently effective triage tools for distinguishing between transient HPV infections and clinically relevant hrHPV-induced diseases are lacking, leading to excessive referrals and overtreatment.

What is added by this report?

This is the first large-scale, prospective, multicenter study to evaluate the triage performance of host DNA six-methylation marker assay (ASTN1, DLX1, ITGA4, RXFP3, SOX17, and ZNF671) in women who are hrHPV-positive in China. Compared with HPV genotyping and cytology [≥ atypical squamous cells of undetermined significance (ASCUS)] screening, the six-methylation marker assay demonstrated superior triage performance, with sensitivities of 82.2% and 90.3% and specificities of 92.4% and 84.1% for cervical intraepithelial grade II/III and worse (CIN2+ and CIN3+), respectively. Further subgroup analysis of women <30 years of age revealed its efficacy. The methylation positivity rate increased with the severity of cervical lesions, and the most significant marker was ZNF671. Moreover, the six-methylation marker assay required the fewest colposcopy referrals, with only 1.32 and 2.39 per CIN2+ and CIN3+ cases, respectively, highlighting its strong health and economic advantages. What are the implications for public health practice?

The large number of women with HPV infections in China each year has led to excessive cytological screenings and colposcopy referrals. A feasible triage tool for women who are hrHPV-positive significantly reduces unnecessary medical resource utilization and offers substantial health and economic benefits.

ABSTRACT

Introduction: Effective detection methods to distinguish between transient human papillomavirus (HPV) infection and clinically relevant high-risk HPV (hrHPV)-induced diseases are lacking, leading to excessive referrals and overtreatment. This study evaluated the clinical performance of a host DNA sixmethylation marker panel (*ASTN1*, *DLX1*, *ITGA4*, *RXFP3*, *SOX17*, and *ZNF671*) to triage Chinese women who were hrHPV-positive.

Methods: This prospective multicenter study enrolled women aged 21–65 years with positive hrHPV testing. hrHPV genotyping, cytology, colposcopy, and the six-methylation marker assay were performed. High-grade cervical lesions were defined as histologically confirmed CIN2+. Forest plots analyses were performed to assess the triage performance of the methylation assay.

Results: Of the 1,806 patients recruited from 4 hospitals in China, 1,659 were included. The methylation assay positivity rates were 7.5%, 73.9%, 88.9%, and 100% for CIN1, CIN2, CIN3, and cervical cancer, respectively. The six-methylation marker assay demonstrated sensitivities of 82.2% and 90.3% and specificities of 92.4% and 84.1% for CIN2+ and CIN3+, respectively, which were higher than those of HPV genotype testing and cytology (\ge ASCUS) screening; the areas under the curve for CIN3+ detection were 0.87 (0.84-0.90), 0.68 (0.64-0.72), and 0.64 (0.60-0.69), respectively. The six-methylation marker assay showed the lowest colposcopy referral rate (24.2%) and required the fewest referrals for detection, with 1.32 and 2.39 referrals per CIN2+ and CIN3+ cases, respectively. In women aged <30 years, the six-methylation marker assay had the highest specificity for CIN2+ (95.7%) and a sensitivity and specificity for CIN3+ of 80.8% and 88.9%, respectively. It had the lowest referral rate (17.17%) and colposcopy referrals, with 1.24 and 2.43 per CIN2+ and CIN3+ cases, respectively.

Conclusions: The host DNA six-methylation marker assay is a reliable triage tool for women who are hrHPV-positive, providing evidence supporting the application of methylation markers in China.

Cervical cancer is the second most common gynecological malignancy that causes death among female patients, with approximately 529,800 new cases and 275,100 deaths annually worldwide. Notably, China accounts for 28% of global cases and 50% of new cases in Asia each year, representing 25%-33% of the annual deaths in Asia (1). Persistent infection with hrHPV is considered the primary cause of cervical cancer and its precancerous lesions. However, HPV genotype testing demonstrates a low specificity of only 31.8% for CIN3 and worse (2). This is because most HPV infections are transient and clear naturally, especially in women younger than 30 years, who have regression rates of 60% (3). Therefore, given China's large population and the substantial number of women who test HPV-positive annually, a reliable triage tool for high-grade intraepithelial lesions (HSIL) is urgently needed.

Ideal triage strategies require a balance between safety, sensitivity, specificity, and screening-related burden; however, a consensus on the optimal triage test is lacking. Various triage methods have been proposed, including p16/Ki-67 cytological dual staining and methylation assays. While p16/Ki-67 demonstrates 90% sensitivity for CIN3+, its limited specificity (42%) fails to reduce colposcopy referral rates (4). A meta-analysis showed that the sensitivity and specificity of all methylation assays for CIN3+ were 0.708 and 0.780, respectively (5). Among these, a methylation panel comprising six markers (ASTN1, DLX1, ITGA4, RXFP3, SOX17, and ZNF671) is suitable for application in developing countries due to its superior specificity (88.7%-94.6%) for CIN3+ (3,6). However, data for this methylation panel come only from clinical trials conducted in Western countries, and the prevalence and distribution of HPV genotypes in China differ from those in Western countries, with significantly higher infection rates of HPV52 and HPV58. Furthermore, the applicability of

the positive threshold of this methylation panel to Chinese women and differences in the expression of methylation markers are unclear.

Therefore, this study hypothesized that the methylation pattern in China might be distinct and conducted a prospective multicenter study to evaluate the clinical performance of a host DNA sixmethylation marker panel in Chinese women who were hrHPV-positive. This was the first prospective multicenter study in China with a large sample size to evaluate the feasibility of the six-methylation marker assay as a triage tool for hrHPV-positive women.

Overall, 1,806 women from the colposcopy clinics of 4 hospitals across China underwent HPV genotype testing, cytological screening, methylation assays, and colposcopy between August 2018 and April 2021. The participating institutions included Peking University First Hospital, Nanjing Drum Tower Hospital, Hunan Provincial Maternal and Child Health Care Hospital, and The First Affiliated Hospital of Anhui Medical University, representing 4 different provinces. The inclusion criteria were as follows: 1) women aged 21–65 years with an intact cervix, 2) hrHPV-positive status with available cervical cytology results, and 3) cervical lesions confirmed through colposcopy biopsy. The exclusion criteria were as follows: 1) pregnant, maternal, or lactating women; 2) unwillingness to participate or inability to provide informed consent; and 3) a history of cervical cancer. This study received ethical approval from all 4 participating hospitals (ethics approval numbers: JNFL2020001, 2020-180-04, JNFL2018001, and PJ 2021-02-06).

Samples were obtained by experienced gynecologists using a cervical brush. Cytology screening employed the liquid-based cytology (LBC) method, and the diagnosis was classified into 5 levels according to the 2014 Bethesda System (TBS) criteria. HPV genotype testing performed using fluorescence was quantification PCR, and results were categorized into 2 groups: HPV16/18-positive and positive for the other 12 hrHPV genotypes, i.e., "other-hrHPV positive." Host DNA from LBC samples was heavy sulfitetransformed for methylation analyses. The methylation panel comprised 6 gene markers: DLX1, ASTN1, ITGA4, RXFP3, SOX17, and ZNF671. All procedures were performed according to standardized instructions. ZNF671 was assigned a score of 3 points, while the other 5 methylation markers were assigned 1 point each. The six-methylation marker assay was considered

positive if the cumulative score across all 6 markers was ≥3. All HPV genotyping and methylation assays were conducted in a central laboratory. All women underwent colposcopy, and cervical biopsies were performed based on colposcopic impressions. Cervical lesions were histologically classified as CIN1/2/3 or cervical cancer (CC), while those with normal biopsy results or colposcopic impressions were categorized as "normal."

This study evaluated 5 triage strategies for detecting CIN2+ and CIN3+ in hrHPV-positive women using histopathology as the gold standard. The evaluated strategies were as follows: 1) HPV16/18 genotyping; 2) cytology (\ge ASCUS); 3) six-methylation marker assay; 4) six-methylation marker assay and HPV16/18 coscreening; and 5) six-methylation marker assay and cytology (\ge ASCUS) co-screening. The sensitivity, specificity, positive predictive value (PPV), negative predictive value (NPV), area under the receiver operating characteristic curve (AUC), and forest plots were calculated for each method. Statistical analyses were performed using SPSS (version 26.0, IBM Corp., NY, USA) and R (version 4.1.2, R Core Team, Vienna, Austria). Independent-sample t-tests were used to compare normally distributed continuous data, whereas nonparametric continuous variables were analyzed using the Mann-Whitney test. Categorical variables were assessed using the chi-squared or Fisher's exact test. To compare methylation marker scores among different CIN groups that followed a nonnormal distribution, this study employed the Kruskal-Wallis test, followed by Dunn's test for pairwise comparisons. Two-sided P<0.05 were considered significant.

Finally, 144 cases did not meet the inclusion criteria, and 3 cases were excluded due to unsuccessful methylation detection, resulting in 1,659 cases available for final analysis, as shown in Figure 1. Assessment using a mixed-effects model showed no significant center effect (*P*>0.05) on baseline characteristics or CIN2+/CIN3+ detection rates. Data from all centers were therefore pooled for final analysis. The study flowchart is presented in Figure 1.

The mean patient age was 41.3 years (range: 21–65). Histopathological findings included 320 (19.3%), 184 (11.1%), 162 (9.8%), and 24 (1.4%) cases of CIN1, CIN2, CIN3, and CC, respectively. Among all cases, 37.1% (259/690) were HPV16/18-positive. The methylation assay demonstrated positivity rates of

7.5% (24/320), 73.9% (136/184), 88.9% (144/162), and 100% (24/24) for CIN1, CIN2, CIN3, and CC, respectively. The methylation scores increased significantly with the severity of cervical lesions (P<0.05). Characteristics of the CC screening and methylation assays are presented in Table 1.

The 3 most frequently positive methylation markers in the CIN2+ and CIN3+ groups were *ZNF671* (65.8% vs. 88.2%), *DLX1* (43.5% vs. 68.3%), and *ASTN1* (37% vs. 61.3%). In the CIN1 group, *DLX1* showed the highest positivity rate (21.6%). However, as the cervical lesions progressed in severity from CIN1 to CIN2, the positive methylation rate of *ZNF671* increased dramatically by 59.2%, which was substantially higher than that of the other markers (Supplementary Table S1, available at https://weekly.chinacdc.cn/). The proportion of samples testing positive for all 6 markers increased from 2.3% in CIN1 to 11.4% in CIN2 and 24.1% in CIN3+. The mean numbers of positive markers in the CIN2, CIN3, and CC groups were 2.5, 3.5, and 4.6, respectively.

The six-methylation marker assay as a single triage tool demonstrated a sensitivity of 82.2% for CIN2+ and a specificity of 92.4%. This sensitivity was significantly higher than that of HPV16/18 genotyping but comparable to that of cytology (≥ASCUS), while its specificity was the highest among all 3 methods. For CIN3+, the six-methylation marker assay achieved a sensitivity of 90.3% and a specificity of 84.1% (Table 2).

The AUCs of HPV16/18 genotyping, cytology (≥ ASCUS), and the six-methylation marker assay for CIN2+ and CIN3+ were 0.61 and 0.64, 0.69 and 0.68, and 0.87 and 0.87, respectively. Combining the six-methylation marker assay with HPV16/18 genotyping (≥ one positive) as a triage tool for CIN2+/3+ resulted in a higher sensitivity but a lower specificity compared to HPV16/18 genotyping alone. The relative sensitivity and specificity with HPV16/18 genotyping and cytology (≥ASCUS) as the reference strategy for CIN2+ and CIN3+ are shown in Figures 2 and 3.

This study further analyzed the efficacy of different triage tools in women aged <30 years. The DNA methylation positivity rate among women who were <30 years of age and hrHPV-positive was 17.2% (51/297), which was lower than that among women >30 years of age (25.8%). The combination of the sixmethylation marker assay and cytology had the highest

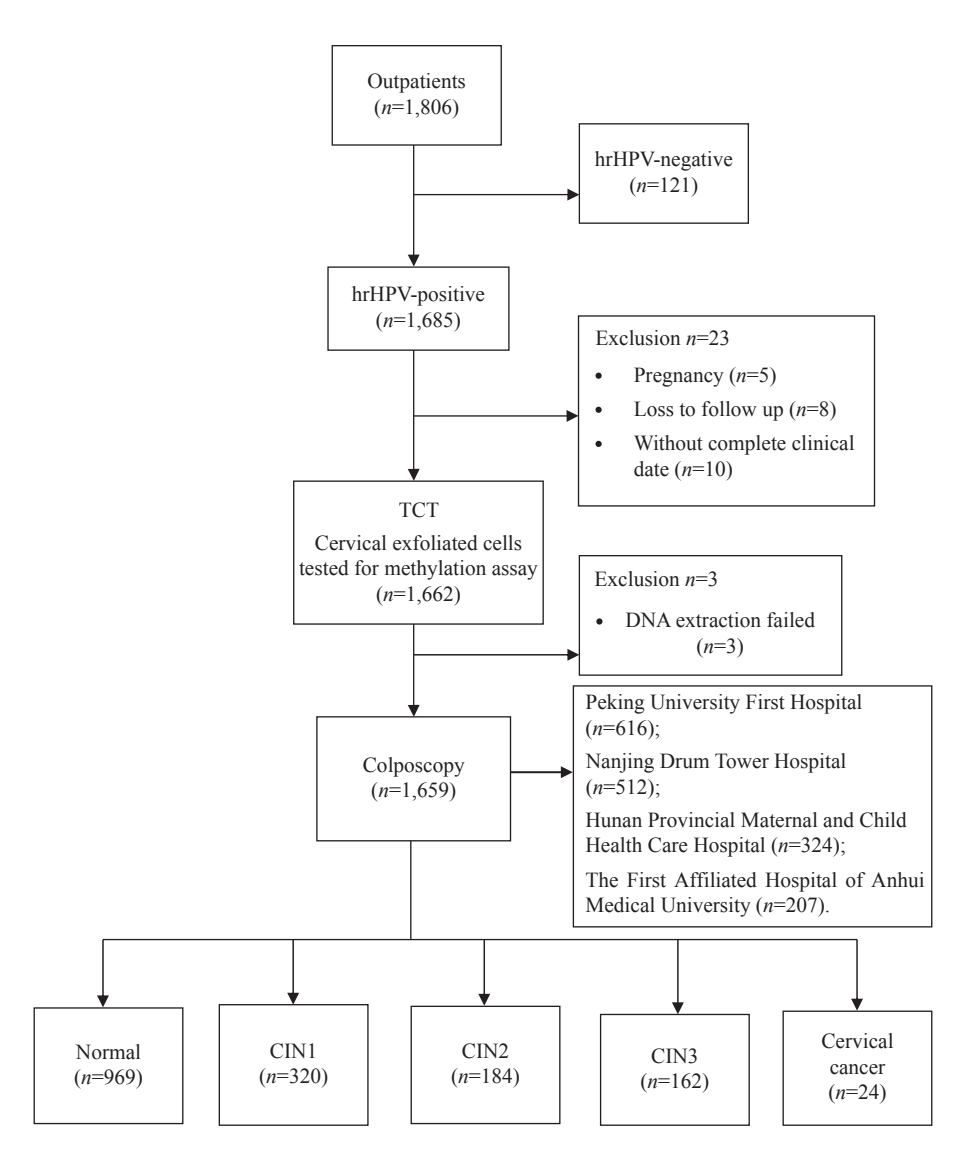


FIGURE 1. Study flowchart of women who were hrHPV-positive.

Abbreviation: HPV=human papillomavirus; TCT=ThinPrep Cytologic Test; CIN=cervical intraepithelial neoplasia.

sensitivity for CIN2+ (89.2%). However, the sixmethylation marker assay showed the highest specificity (95.7%), with relative specificities of 1.34 and 1.8 compared to HPV genotyping and cytology (≥ ASCUS), respectively. For CIN3+ detection, the sixmethylation marker assay demonstrated relatively good sensitivity and specificity, with values of 80.8% and 88.9%, respectively (Supplementary Table S2, available at https://weekly.chinacdc.cn/). Notably, it also demonstrated the highest specificity among the 5 triage strategies in the overall cohort for the detection of CIN2+ or CIN3+, particularly in the subgroup analysis of women <30 years of age for CIN2+ (Table 2 and Supplementary Table S2).

In addition, the six-methylation marker assay demonstrated the lowest colposcopy referral rate

(24.23%) and the fewest referrals required for detection, with 1.32 and 2.39 referrals per CIN2+ and CIN3+ cases, respectively. In contrast, HPV16/18 genotyping and cytology (≥ASCUS) required approximately 3 referrals each per CIN2+ case, and 5.02 and 5.61 referrals per CIN3+ case, respectively. In the subgroup analysis of women <30 years of age, the six-methylation marker assay also demonstrated the lowest colposcopy referral rates (17.17%) and colposcopy referrals (Supplementary Table S3, available at https://weekly.chinacdc.cn/).

DISCUSSION

Due to China's large population, many women who are hrHPV-positive require annual colposcopy

TABLE 1. Cervical screening and six-methylation marker assay for cervical precancerous lesions and cervical cancer.

Items	Normal	CIN1	CIN2	CIN3	CC	Total	P
Number (n, %)	969 (58.4)	320 (19.3)	184 (11.1)	162 (9.8)	24 (1.4)	1,659	_
Age (years, mean±SD)	42.6±10.5	38.9±10.4	39.6±9.8	42.2±10.3	41.2±10.1	41.3±10.4	0.69
hrHPV results (n, %)							
HPV 16/18	291 (30.0)	70 (21.9)	77 (41.8)	89 (54.9)	20 (83.3)	547 (33.0)	0.04*
Other-hrHPV	678 (70.0)	250 (78.1)	107 (58.2)	73 (45.1)	4 (16.7)	1,112 (67.0)	0.01*
Cytology results (n, %)							
Normal	576 (59.4)	118 (36.9)	36 (19.6)	23 (14.2)	2 (8.3)	755 (45.5)	40 004*
≥ASCUS	393 (40.6)	202 (63.1)	148 (80.4)	139 (85.8)	22 (91.7)	904 (54.5)	<0.001*
Methylation (n, %)							
Positive	74 (7.6)	24 (7.5)	136 (73.9)	144 (88.9)	24 (100)	402 (24.2)	-0.004*
Negative	895 (92.4)	296 (92.5)	48 (26.1)	18 (11.1)	0 (0)	1,257 (75.8)	<0.001*
Score (mean±SD)	0.6±1.3	0.60±1.4	3.6±2.5	4.6±2.2	5.7±2.4	1.5±2.3	<0.001*
Methylation in women <30	years of age (n, %	%)					
Positive	4 (2.8)	6 (6.7)	20 (51.3)	16 (76.2)	5 (100.0)	51 (17.2)	<0.01*
Negative	138 (97.2)	84 (93.3)	19 (48.7)	5 (23.8)	0 (0)	246 (82.8)	
Score (mean±SD)	0.9±1.2	1.4±2.4	1.4±2.1	2.0±2.6	2.6±3.4	1.3±2.2	0.04*

Note: "-" means "Not Applicable".

Abbreviation: HPV=human papillomavirus; CIN=cervical intraepithelial neoplasia; CC=cervical cancer; ASCUS=atypical squamous cells of undetermined significance; SD=standard deviation.

TABLE 2. Performance of different triage tools for the detection of CIN2+/CIN3+ among women who were hrHPV-positive.

	Sensitivity (%) Specificity (%)				Compared w	ith HPV16/18	Compared with cytology	
Triage algorithms	n/N 95% CI	n/N 95% CI	PPV (%) n/N 95% CI	NPV (%) n/N 95% CI	Relative sensitivity (95% CI)	Relative specificity (95% CI)	Relative sensitivity (95% CI)	Relative specificity (95% CI)
For CIN2+								
HPV16/18	50.3 (45.2–55.4)	72.0 (69.5–74.4)	34.0 (30.0–38.0)	83.5 (81.3–85.6)	1.00	1.00	0.60 (0.54–0.66)	1.34 (1.29–1.38)
Cytology (≥ASCUS)	83.5 (79.7–87.3)	53.8 (51.1–56.6)	34.2 (31.1–37.3)	91.9 (90.0–93.9)	1.66 (1.58–1.74)	0.75 (0.71–0.79)	1.00	1.00
Methylation	82.2 (78.3–86.1)	92.4 (91.0–93.8)	75.6 (71.4–79.8)	94.7 (9.3.5–96.0)	1.63 (1.56–1.71)	1.28 (1.26–1.30)	0.98 (0.94–1.03)	1.72 (1.69–1.74)
Methylation or HPV16/18 Methylation or cytology	` 92.2 ´	67.5 (64.9–70.1) 50.3 (47.6–53.1)	44.9 (41.3–48.4) 35.4 (32.4–38.3)	96.8 (95.6–97.9) 97.0 (95.7–98.3)	1.83 (1.78–1.89) 1.88 (1.83–1.93)	0.94 (0.90–0.97) 0.70 (0.66–0.74)	1.10 (1.07–1.14) 1.13 (1.11–1.16)	1.25 (1.21–1.30) 0.93 (0.88–0.99)
For CIN3+								
HPV16/18	58.6 (51.5–65.7)	70.3 (67.9–72.6)	19.9 (16.6–23.3)	93.1 (91.6–94.6)	1.00	1.00	0.68 (0.59–0.76)	1.42 (1.37–1.46)
Cytology (⊵ASCUS)	86.6 (81.7–91.5)	49.6 (47.0–52.1)	17.8 (15.3–20.3)	96.7 (95.4–98.0)	1.48 (1.39–1.56)	0.71 (0.67–0.74)	1.00	1.00
Methylation	90.3 (86.1–94.6)	84.1 (82.2–86.0)	41.8 (37.0–46.6)	98.6 (97.9–99.2)	1.54 (1.47–1.61)	1.20 (1.17–1.27)	1.04 (0.99–1.09)	1.70 (1.66–1.73)
Methylation	96.8	60.6	23.7	99.3	1.65	0.86	1.12	1.22
or HPV16/18 Methylation	96.8 (94.2–99.3) (94.2–99.3)	(58.1–63.1) 45.0 (42.5–47.6)	(20.7–26.7) 18.2 (15.8–20.6)	(98.8–99.9) 99.1 (98.4–99.8)	(1.61–1.69) 1.65 (1.61–1.69)	(0.83–0.90) 0.64 (0.60–0.68)	(1.09–1.15) 1.12 (1.09–1.15)	(1.17–1.27) 0.91 (0.86–0.96)
or cytology	(34.2-33.3)	(42.5-47.0)	(13.0-20.0)	(30.4-33.0)	(1.01-1.09)	(0.00-0.00)	(1.03-1.13)	(0.00-0.90)

Abbreviation: PPV=positive predictive value; NPV=negative predictive value; AUC=area under the receiver operating characteristic curve; HPV=human papillomavirus; ASCUS=atypical squamous cells of undetermined significance; CI=confidence interval.

referrals. Currently, the main triage techniques used for women who are hrHPV-positive in China are cytology and hrHPV genotype testing. However, cytology has a relatively low sensitivity (50%–70%) for HSIL detection (7), and hrHPV genotype testing cannot distinguish between transient and persistent HPV

^{*} P<0.05.

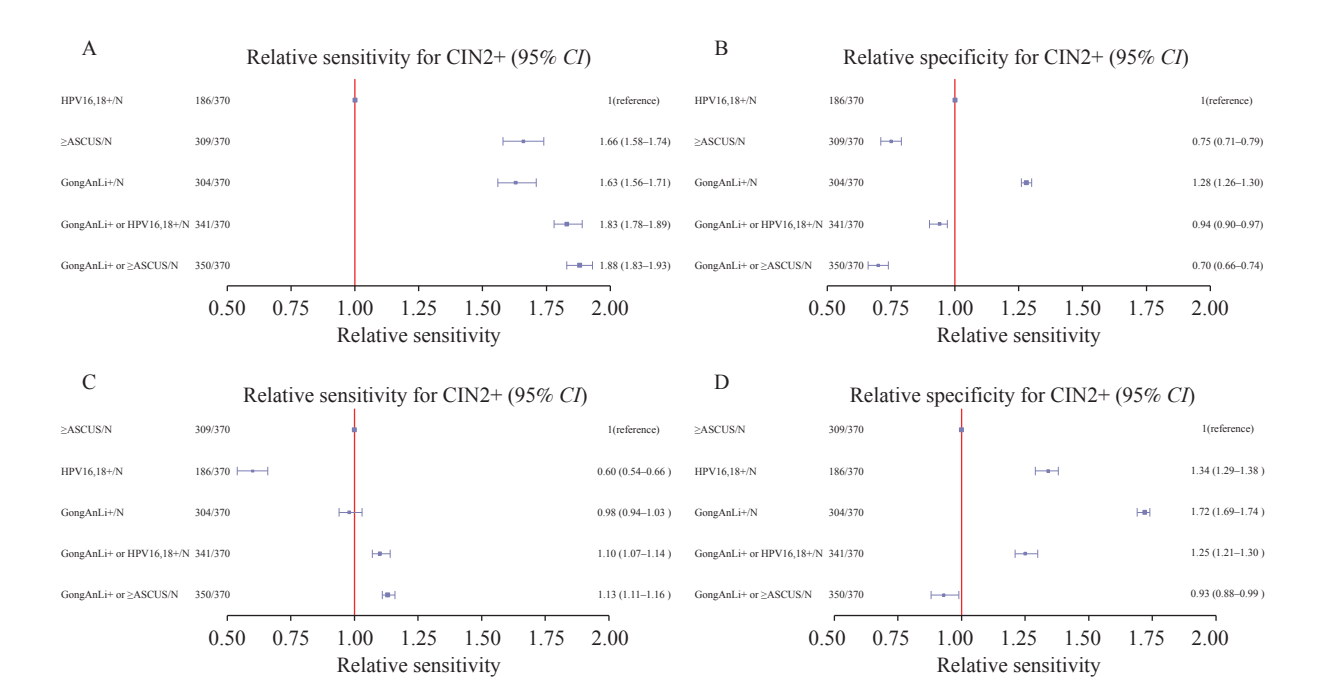


FIGURE 2. Forest plots showing the relative sensitivity and specificity for CIN2+ detection of different triage tools compared with HPV16/18 genotyping and cytology (\geq ASCUS). The relative (A) sensitivity and (B) specificity of different triage tools compared with HPV16/18 genotyping; The relative (C) sensitivity and (D) specificity of different triage tools compared with cytology (\geq ASCUS).

Abbreviation: CIN2+=cervical intraepithelial neoplasia grade 2 or worse; HPV=human papillomavirus; ASCUS=atypical squamous cells of undetermined significance.

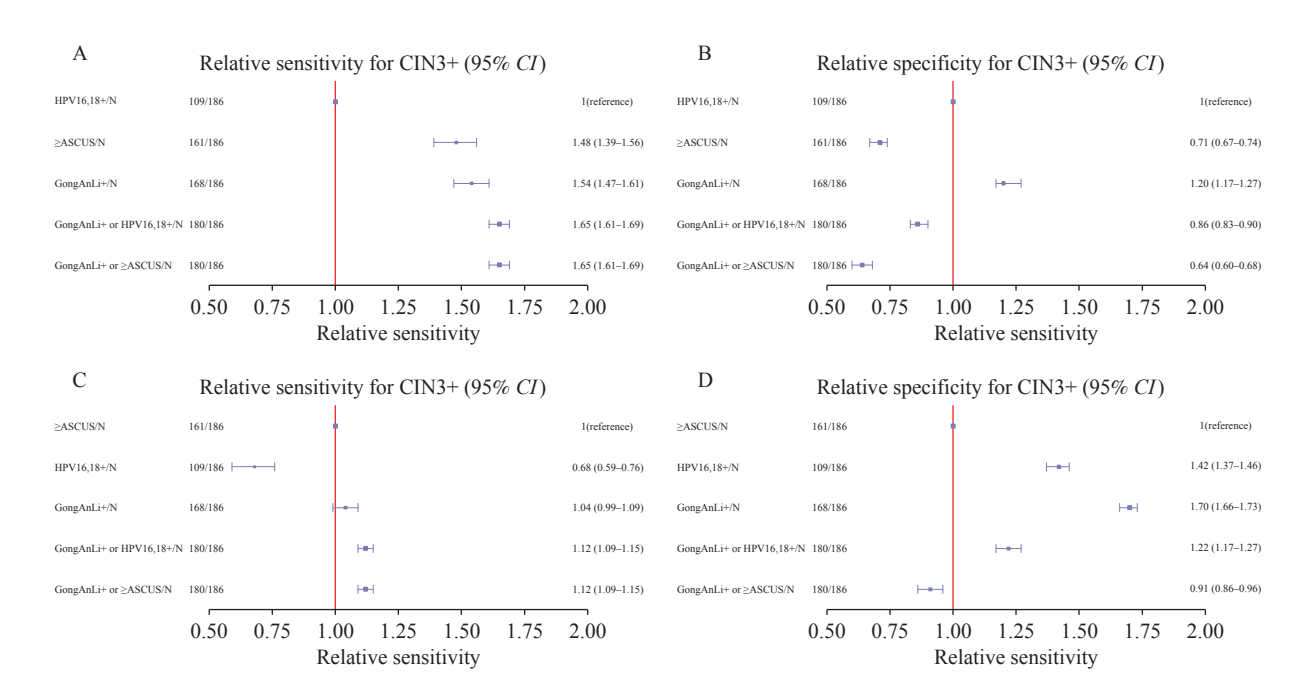


FIGURE 3. Forest plots showing the relative sensitivity and specificity for CIN3+ detection of different triage tools compared with HPV 16/18 genotyping and cytology (≥ASCUS). (A) The relative sensitivity of different triage tools compared with HPV 16/18 genotyping; (B) The relative specificity of different triage tools compared with HPV 16/18 genotyping; (C) The relative sensitivity of different triage tools compared with cytology (≥ASCUS); (D) The relative specificity of different triage tools compared with cytology (≥ASCUS).

Abbreviation: CIN2+=cervical intraepithelial neoplasia grade 2 or worse; HPV=human papillomavirus; ASCUS=atypical squamous cells of undetermined significance.

infections, all resulting in clinical overtreatment.

Consequently, numerous DNA methylation genes have been reported as promising markers for HSIL detection. Sofia et al. conducted a meta-analysis of 23 studies examining DNA methylation-based biomarkers in women who are hrHPV-positive (8) and found that DNA methylation assays demonstrated a sensitivity of 0.78 (95% CI: 0.74-0.82) and specificity of 0.74 (95% CI: 0.69–0.78) for CIN3+. The previous methylation assay comprising 6 markers (ASTN1, DLX1, ITGA4, RXFP3, SOX17, and ZNF671) in Germany has been implemented clinically with a sensitivity of 67.7% (95% CI: 57.3%-77.1%) and specificity of 88.7% (95% CI: 83.7%-92.6%) for CIN3+ (3) and shows a much higher specificity than another assay that simultaneously detects p16 and Ki-67 immunocytochemistry (6). However, it has not been recommended by WHO guidelines (9) and requires additional clinical research to verify its value. Furthermore, its applicability in Chinese women remains unknown.

To this study's knowledge, this is the first prospective multicenter study, and is using the largest cohort, to evaluate a six-methylation marker panel in women who are hrHPV-positive. Although this study's methylation panel shared the same 6 gene markers as a previous methylation panel from Germany, the scoring algorithms differed significantly. The threshold for the previous methylation panel was 0.5, with individual marker contributions as follows: DLX1 (0.1), ASTN1 (0.2), ITGA4 (0.2), RXFP3 (0.2), SOX17 (0.2), and ZNF671 (0.5); the cutoff value of the six-methylation marker panel in this study was 3. This finding may correlate with the variations in HPV genotype prevalence and distribution between Chinese and Western women, suggesting that Chinese women may exhibit different DNA methylation patterns. Nevertheless, this study confirmed that this sixmethylation marker panel demonstrated significantly higher sensitivity and specificity for CIN3+ compared to HPV genotyping and cytology (\ge ASCUS), supporting its potential as a reliable triage tool.

Previous studies have predominantly focused on evaluating the triage efficacy of methylation assays for CIN3+, with limited attention given to CIN2. However, CIN2 has a higher regression rate in clinical practice, especially in young women (<30 years of age) (3). Dippmann et al. compared the performance of the six-methylation marker assay with that of the QIAsure

Methylation Test using 195 cervical scrapes from Western countries (1) and found that the sixmethylation marker assay exhibited significantly higher specificity for CIN2+ (87.6% vs. 67.4%; P<0.001). In another study involving 396 cervical lesions, the specificity of the six-methylation marker assay for CIN2+ was 51.6%, which was higher than those of both HPV genotype testing (21.5%) and cytology (≥ ASCUS) (45.2%) (10). In contrast to prior smallsample studies, this large-scale, prospective, multicenter study further validated the reliable triage performance of the six-methylation marker assay for CIN2+, even in women <30 years of age, which had the highest specificity and provided critical evidence to guide the clinical management of women with CIN2+. These findings align with those reported by Vink et al., who found that the FAM19A4/miR124-2 Methylation Test provided superior specificity compared to HPV16/18 genotyping for CIN2/3 detection in women aged <30 years (11). This suggests that followup without immediate intervention may be safe for who are methylation-negative. young women However, these hypotheses warrant investigation.

Furthermore, this study found that the positivity rate of the six-methylation marker assay significantly lower in young women. This agedependent detection rate was confirmed in another study using a six-methylation marker assay in Western countries, although in that study, only 30% of women <30 years of age with CIN2/3 were methylationpositive compared to 70% in the older group (P=0.004) (1). This may be related to the high prevalence of transient HPV infections and higher regression rates of CIN2 lesions in younger women. This study also analyzed the methylation levels of six methylation markers and found that ZNF671 had the highest positivity rate (81.6%) in patients who were with CIN3+. Another real-time methylation-specific PCR analysis of ZNF671 showed the highest detection rates for cervical scrapes with CIN3 (71%) and cancer (97.3%) (10), and the ZNF671 methylation test showed superior performance compared to PAX1 for CIN3+ detection (12). This finding suggests that ZNF671 plays a particularly important role in the positive determination of methylation assays for HSIL detection. Additionally, this study observed that the methylation DNA positivity rates methylation scores in women with CIN1 and without CIN were similar and significantly lower than those in women with CIN2+ and CIN3+. This indicates that the DNA methylation assay can effectively distinguish patients with HSIL from women without HSIL.

This study also assessed cost-effectiveness by comparing the colposcopy referral rates across five triage strategies. The six-methylation marker assay performed best in both the overall population and in younger women who were hrHPV-positive, suggesting its potential to reduce CC screening costs, minimize unnecessary colposcopies, and lower the national healthcare burden while decreasing patient discomfort and infection risks from repeated procedures.

In conclusion, the host DNA six-methylation marker assay demonstrated relatively superior triage performance for both overall and young (<30 years) women who were hrHPV-positive, significantly reducing colposcopy referrals and making it a costeffective and reliable triage strategy. Based on this study's findings, its authors hypothesize that the host DNA six-methylation marker assay may serve as an alternative to cytology, particularly for women who are hrHPV-positive and have ASCUS/LSIL (Low-grade Squamous Intraepithelial Lesion) cytology or non-16/18 HPV genotypes in regions with limited availability of cytologists or colposcopists. implementation may reduce reliance on cytology quality and minimize unnecessary colposcopies and overtreatment. Further prospective studies are required to validate the feasibility of these clinical applications.

The findings in this report are subject to at least four limitations. First, cervical lesions were not followed-up long term. Although the methylation assay serves as a crucial tool for investigating HPV integration into the host DNA, it cannot directly differentiate between persistent and transient HPV infections. Long-term follow-up is required to further elucidate the relationships among methylation, HPV infection, and persistent CIN lesion. Second, although methylation testing reduces false-positive costs, the technical complexity and infrastructure requirements pose challenges for implementation in resource-limited settings, necessitating standardized protocols and training programs. Third, to minimize analytical variability, HPV genotyping and methylation assays were conducted in a central laboratory; however, potential confounding factors include inter-center differences in cytology interpretation and colposcopy practices and sample selection bias. Finally, this study focused exclusively on women who were hrHPV-positive, and the findings may not be generalizable to women who are HPV-negative or populations without prior HPV screening, highlighting the need for larger cohort studies to refine these results.

Conflicts of interest: No conflicts of interest.

Acknowledgements: All the participants in this study.

doi: 10.46234/ccdcw2025.230

Copyright © 2025 by Chinese Center for Disease Control and Prevention. All content is distributed under a Creative Commons Attribution Non Commercial License 4.0 (CC BY-NC).

Submitted: July 10, 2025 Accepted: August 25, 2025 Issued: October 24, 2025

REFERENCES

- Dippmann C, Schmitz M, Wunsch K, Schütze S, Beer K, Greinke C, et al. Triage of hrHPV-positive women: comparison of two commercial methylation-specific PCR assays. Clin Epigenet 2020;12(1):171. https://doi.org/10.1186/s13148-020-00963-w.
- Leeman A, Del Pino M, Marimon L, Torné A, Ordi J, Ter Harmsel B, et al. Reliable identification of women with CIN3+ using hrHPV genotyping and methylation markers in a cytology-screened referral population. Int J Cancer 2019;144(1):160 – 8. https://doi.org/10.1002/ ijc.31787.
- 3. Schmitz M, Wunsch K, Hoyer H, Scheungraber C, Runnebaum IB, Hansel A, et al. Performance of a methylation specific real-time PCR assay as a triage test for HPV-positive women. Clin Epigenet 2017;9(1): 118. https://doi.org/10.1186/s13148-017-0419-2.
- McMenamin M, McKenna M, McDowell A. Clinical utility of CINtec PLUS triage in equivocal cervical cytology and human papillomavirus primary screening. Am J Clin Pathol 2018;150(6):512 – 21. https://doi. org/10.1093/ajcp/aqy073.
- Yue X, Duan YQ, Guo DJ, Wang YX, Wang CP, Liu X. Diagnostic accuracy of available methylation assays in advanced cervical intraepithelial neoplasia from high-risk HPV-positive women: a systematic review and network *meta*-analysis. Eur J Obstet Gynecol Reprod Biol 2025;308:54 – 65. https://doi.org/10.1016/j.ejogrb.2025. 02.038.
- Schmitz M, Eichelkraut K, Schmidt D, Zeiser I, Hilal Z, Tettenborn Z, et al. Performance of a DNA methylation marker panel using liquidbased cervical scrapes to detect cervical cancer and its precancerous stages. BMC Cancer 2018;18(1):1197. https://doi.org/10.1186/ s12885-018-5125-8.
- Cuzick J, Clavel C, Petry KU, Meijer CJLM, Hoyer H, Ratnam S, et al. Overview of the European and North American studies on HPV testing

^{*} Corresponding author: Yan Zhang, zhangyan66@bjmu.edu.cn.

Department of Gynecology and Obstetrics, Peking University First Hospital, Beijing, China; ² Peking University Health Science Center, Beijing, China; ³ Department of Gynecology and Obstetrics, Nanjing Drum Tower Hospital, Nanjing City, Jiangsu Province, China; ⁴ Department of Gynecology and Obstetrics, Hunan Provincial Maternal and Child Health Care Hospital; Changsha City, Hunan Province, China; ⁵ Department of Gynecology and Obstetrics, The First Affiliated Hospital of Anhui Medical University, Hefei City, Anhui Province, China.

[&]amp; Joint first authors.

China CDC Weekly

- in primary cervical cancer screening. International Journal of Cancer. 2006;119(5):1095 1101 https://doi.org/10.1002/ijc.21955.
- Salta S, Lobo J, Magalhães B, Henrique R, Jerónimo C. DNA methylation as a triage marker for colposcopy referral in HPV-based cervical cancer screening: a systematic review and meta-analysis. Clin Epigenet 2023;15(1):125. https://doi.org/10.1186/s13148-023-01537-2.
- 9. World Health Organization. WHO guideline for screening and treatment of cervical pre-cancer lesions for cervical cancer prevention. 2nd ed. Geneva: World Health Organization. 2021. https://www.who.int/publications/i/item/9789240030824.
- 10. Shi LY, Yang X, He L, Zheng CY, Ren Z, Warsame JA, et al. Promoter hypermethylation analysis of host genes in cervical intraepithelial

- neoplasia and cervical cancers on histological cervical specimens. BMC Cancer 2023;23(1):168. http://dx.doi.org/10.1186/s12885-023-10628-5.
- Vink FJ, Meijer CJLM, Hesselink AT, Floore AN, Lissenberg-Witte BI, Bonde JH, et al. FAM19A4/miR124-2 methylation testing and human papillomavirus (HPV) 16/18 genotyping in HPV-positive women under the age of 30 years. Clin Infect Dis 2023;76(3):e827 – 34. https://doi.org/10.1093/cid/ciac433.
- Zhu P, Xiong J, Yuan D, Li X, Luo LL, Huang J, et al. ZNF671 methylation test in cervical scrapings for cervical intraepithelial neoplasia grade 3 and cervical cancer detection. Cell Rep Med 2023;4 (8):101143. https://doi.org/10.1016/j.xcrm.2023.101143.

SUPPLEMENTARY MATERIAL

SUPPLEMENTARY TABLE S1. Positivity rates of methylation markers in precancerous and cancerous cervical lesions.

Methylation marker	F	Positivity rate (%, r	Differen				
wetnylation marker	CIN1+ (n=320)	CIN2+ (n=184)	CIN3+ (n=186)	Δ1	Δ2	Δ3	— Р
ASTN1	7.2 (23)	37.0 (68)	61.3 (114)	29.8	24.3	54.1	<0.05*
DLX1	21.6 (69)	43.5 (80)	68.3 (127)	21.9	24.8	46.7	<0.05*
ITGA4	3.1 (10)	26.1 (48)	43.5 (81)	23.0	17.4	40.4	<0.05*
RXFP3	4.4 (14)	23.4 (43)	40.3 (75)	23.0	12.9	35.9	<0.05*
SOX17	4.4 (14)	33.7 (62)	53.2 (99)	29.3	19.5	48.8	<0.05*
ZNF671	6.6 (21)	65.8 (121)	88.2 (164)	59.2	22.4	81.6	<0.05*
Methylation	7.5 (24)	73.9 (136)	90.3 (168)	66.4	16.4	82.8	<0.05*

Note: Δ1=Difference in positivity rates between CIN2+ and CIN1+ (CIN2+ – CIN1+); Δ2=Difference in positivity rates between CIN3+ and CIN2+ (CIN3+ – CIN2); Δ3=Difference in positivity rates between CIN3+ and CIN1 (CIN3+ – CIN1+).

SUPPLEMENTARY TABLE S2. Performance of different triage tools in the detection of CIN2+/CIN3+ in women aged <30 years who are hrHPV-positive.

	Sensitivity (%) Specificity (%) (95% CI) (95% CI)				Compared w	ith HPV 16/18	Compared with cytology	
Triage algorithms			PPV (%) (95% CI)	NPV (%) (95% CI)	Relative sensitivity (95% CI)	Relative specificity (95% CI)	Relative sensitivity (95% CI)	Relative specificity (95% CI)
For CIN2+								
HPV16/18	53.9 (48.2-59.5)	71.6 (66.4–76.7)	34.7 (29.2–40.1)	84.7 (80.6–88.8)	1.00	1.00	0.66 (0.51, 0.85)	1.35 (1.17, 1.56)
Cytology (≥ASCUS)	81.5 (77.1–86.0)	53.0 (47.3–58.7)	32.7 (27.4–38.1)	91.1 (87.9–94.4)	1.51 (1.18, 1.95)	0.74 (0.64, 0.86)	1.00	1.00
Methylation	63.1 (57.6–68.6)	95.7 (93.4–98.0)	80.4 (75.9–84.9)	90.2 (86.9–93.6)	1.17 (0.87, 1.57)	1.34 (1.23, 1.46)	0.77 (0.62, 0.96)	1.80 (1.59, 2.04)
Methylation or HPV16/18 Methylation or cytology	` 84.6	69.0 (63.7–74.2) 50.9 (45.2–56.6)	43.3 (37.7–48.9) 33.7 (28.3–39.1)	94.1 (91.4–96.8) 94.4 (91.8–97.0)	1.57 (1.23, 2.01) 1.66 (1.30, 2.11)	0.96 (0.86, 1.09) 0.71 (0.61, 0.83)	1.04 (0.89, 1.21) 1.09 (0.95, 1.26)	1.30 (1.12, 1.51) 0.96 (0.81, 1.14)
For CIN3+	,	,	,	,	, ,	, ,	, ,	, ,
HPV16/18	65.4 (60.0–70.8)	69.0 (63.7–74.3)	16.8 (12.6–21.1)	95.4 (93.0–97.8)	1.00	1.00	0.81 (0.58, 1.13)	1.44 (1.24, 1.67)
Cytology (≥ASCUS)	80.8 (76.3–85.3)	48.0 (42.3–53.7)	13.0 (9.1–16.8)	96.3 (94.2–98.4)	1.24 (0.88, 1.73)	0.70 (0.60, 0.81)	1.00	1.00
Methylation	80.8 (76.3–85.3)	88.9 (85.4–92.5)	41.2 (35.6–46.8)	98.0 (96.4–99.6)	1.24 (0.88, 1.73)	1.29 (1.21, 1.33)	1.00 (0.77, 1.30)	1.85 (1.63, 2.11)
Methylation	92.3	62.0	18.9	98.8	1.41	0.90	1.14	1.29
or HPV16/18	,	(56.5–67.5)	(14.5–23.4)	(97.6–100.0)	(1.04, 1.91)	(0.79, 1.02)	(0.92, 1.42)	(1.11, 1.51)
Methylation or cytology	88.5 (84.8–92.1)	45.0 (39.4–50.7)	13.4% (9.5–17.2)	97.6% (95.9–99.3)	1.35 (0.99, 1.85)	0.65 (0.56, 0.76)	1.10 (0.87, 1.38)	0.94 (0.78, 1.12)

Abbreviation: PPV=positive predictive value; NPV=negative predictive value; AUC=area under the receiver operating characteristic curve; C/=confidence interval.

Abbreviation: CIN=cervical intraepithelial neoplasia; CIN2+=cervical intraepithelial neoplasia grade 2 or worse.

^{*} P<0.05.

China CDC Weekly

SUPPLEMENTARY TABLE S3. Referral rates and number of referrals needed to detect one CIN2+/CIN3+ case.

Triage algorithms	CIN2+ cases detected (n)	CIN3+ cases detected (n)	Referrals to colposcopy (n)	Referral rate (%)	Referrals needed to detect 1 CIN2+ case (%)	Referrals needed to detect 1 CIN3+ case (%)
All women who were hrHPV-pos	sitive					
HPV16/18	186	109	547	32.97	2.94	5.02
Cytology (≥ASCUS)	309	161	904	54.49	2.93	5.61
Methylation	304	168	402	24.23	1.32	2.39
Methylation or HPV16/18	341	180	760	45.81	2.23	4.22
Methylation or cytology	350	180	990	59.67	2.83	5.50
Women <30 years of age						
HPV16/18	35	17	101	34.01	2.89	5.94
Cytology (≥ASCUS)	53	21	162	54.55	3.06	7.71
Methylation	41	21	51	17.17	1.24	2.43
Methylation or HPV16/18	55	24	127	42.76	2.31	5.29
Methylation or cytology	58	23	172	57.91	2.97	7.48

Abbreviation: HPV=human papillomavirus; CIN=cervical intraepithelial neoplasia; ASCUS=atypical squamous cells of undetermined significance.

Youth Editorial Board

Director Lei Zhou

Vice Directors Jue Liu Tiantian Li Tianmu Chen

Members of Youth Editorial Board

Jingwen Ai Li Bai Yuhai Bi Yunlong Cao Gong Cheng Liangliang Cui Meng Gao Jie Gong Yuehua Hu Xiang Huo Jia Huang Xiaolin Jiang Yu Ju Min Kang Huihui Kong Lingcai Kong Shengjie Lai Fangfang Li Jingxin Li **Huigang Liang** Di Liu Jun Liu Li Liu Yang Liu Chao Ma Yang Pan Zhixing Peng Menbao Qian Tian Qin Shuhui Song Kun Su Song Tang Bin Wang Jingyuan Wang Linghang Wang Qihui Wang Feixue Wei Xiaoli Wang Xin Wang Yongyue Wei Zhiqiang Wu Meng Xiao Tian Xiao Wuxiang Xie Lei Xu Lin Yang Canging Yu Lin Zeng Yi Zhang Yang Zhao Hong Zhou

Indexed by Science Citation Index Expanded (SCIE), Social Sciences Citation Index (SSCI), PubMed Central (PMC), Scopus, Chinese Scientific and Technical Papers and Citations, and Chinese Science Citation Database (CSCD)

Copyright © 2025 by Chinese Center for Disease Control and Prevention

Under the terms of the Creative Commons Attribution-Non Commercial License 4.0 (CC BY-NC), it is permissible to download, share, remix, transform, and build upon the work provided it is properly cited. The work cannot be used commercially without permission from the journal. References to non-China-CDC sites on the Internet are provided as a service to CCDC Weekly readers and do not constitute or imply endorsement of these organizations or their programs by China CDC or National Health Commission of the People's Republic of China. China CDC is not responsible for the content of non-China-CDC sites.

The inauguration of *China CDC Weekly* is in part supported by Project for Enhancing International Impact of China STM Journals Category D (PIIJ2-D-04-(2018)) of China Association for Science and Technology (CAST).



Vol. 7 No. 43 Oct. 24, 2025

Responsible Authority

National Disease Control and Prevention Administration

Sponsor

Chinese Center for Disease Control and Prevention

Editing and Publishing

China CDC Weekly Editorial Office No.155 Changbai Road, Changping District, Beijing, China Tel: 86-10-63150501, 63150701 Email: weekly@chinacdc.cn

CSSN

ISSN 2096-7071 (Print) ISSN 2096-3101 (Online) CN 10-1629/R1